

He-like ions as practical astrophysical plasma diagnostics: From stellar coronae to active galactic nuclei

D. Porquet · J. Dubau · N. Grosso

Received: date / Accepted: date

Abstract We review X-ray plasma diagnostics based on the line ratios of He-like ions. Triplet/singlet line intensities can be used to determine electronic temperature and density, and were first developed for the study of the solar corona. Since the launches of the X-ray satellites Chandra and XMM-Newton, these diagnostics have been extended and used (from C V to Si XIII) for a wide variety of astrophysical plasmas such as stellar coronae, supernova remnants, solar system objects, active galactic nuclei, and X-ray binaries. Moreover, the intensities of He-like ions can be used to determine the ionization process(es) at work, as well as the distance between the X-ray plasma and the UV emission source for example in hot stars. In the near future thanks to the next generation of X-ray satellites (e.g., Astro-H and IXO), higher-Z He-like lines (e.g., iron) will be resolved, allowing plasmas with higher temperatures and densities to be probed. Moreover, the so-called satellite lines that are formed closed to parent He-like lines, will provide additional valuable diagnostics to determine electronic temperature, ionic fraction, departure from ionization equilibrium and/or from Maxwellian electron distribution.

Keywords plasma diagnostics · atomic processes · Line: formation · radiation mechanisms: thermal · X-rays: general

Contents

1	Introduction	2
2	Atomic processes and atomic data	5
3	Ionization process diagnostic	8
4	Electronic temperature and density diagnostics	15
5	Satellite lines to He-like ions	23
6	Conclusions and perspectives	27

Delphine Porquet and Nicolas Grosso
Observatoire Astronomique de Strasbourg, Université de Strasbourg, CNRS, UMR 7550,
11 rue de l'Université, F-67000 Strasbourg, France
E-mail: delphine.porquet@astro.unistra.fr, nicolas.grosso@astro.unistra.fr

Jacques Dubau
Institut d'Astrophysique Spatiale, Université Paris Sud-11, F-91405 Orsay Cedex, France
E-mail: jacques.dubau@ias.u-psud.fr

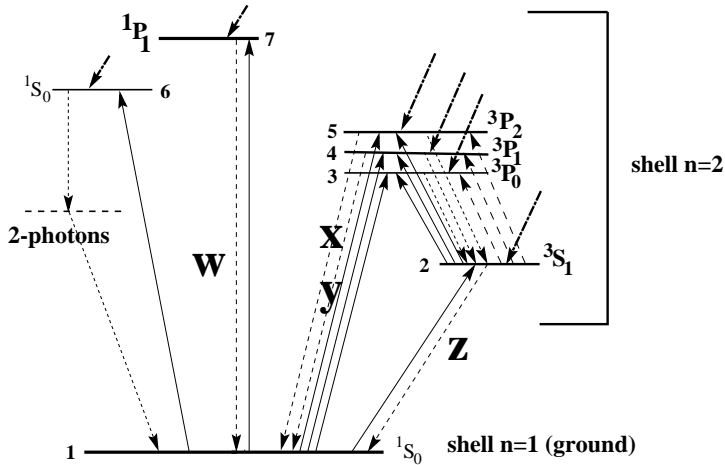


Fig. 1 Simplified level scheme for He-like ions. w (or R), x, y (or I), and z (or F) are the resonance, intercombination, and forbidden lines, respectively. Upward arrows correspond to the electron collisional excitation transitions (solid) and to the photo-excitation from 2^3S_1 to $2^3P_{0,1,2}$ levels (dashed). Downward arrows correspond to the radiative transitions (including 2-photon continuum from 2^1S_0 to the ground level). Thick downward arrows: recombination (radiative and dielectronic) plus cascade processes. Figure from Porquet and Dubau (2000). Courtesy of Astronomy & Astrophysics.

1 Introduction

Spectral lines of H-like and He-like ions are among the most prominent features in X-ray spectra from a large variety of astrophysical sources. Compared to other ionic iso-electronic sequences, He-like ions are abundant over the widest temperature range in collisional plasmas due to their closed shell ground state. The most intense He-like lines correspond to transitions between the $n = 2$ shell and the $n = 1$ ground state shell (see Fig. 1):

- The resonance line, named in the literature either R or w is an electric dipole transition (E1; $1s^2\ ^1S_0 - 1s2p\ ^1P_1$);
- The intercombination line I is composed of two lines x (M2: magnetic quadrupole transition; $1s^2\ ^1S_0 - 1s2p\ ^3P_2$) and y (E1; $1s^2\ ^1S_0 - 1s2p\ ^3P_1$). The quadrupole line x only becomes intense for He-like ions heavier than S xv, and with the same intensity as the line y for Ca xix. The transition from 3P_0 cannot decay to the ground level since this transition is strictly forbidden but decays to the 3S_1 metastable level.
- The forbidden line F or z is a relativistic magnetic dipole transition (M1; $1s^2\ ^1S_0 - 1s2s\ ^3S_1$).

The $1s2s\ ^1S_0$ level decays to the ground level by a two-photon process (see section 2). The energies and wavelengths of these lines for C v ($Z=6$), N vi, O vii, Ne ix, Mg xi, Si xiii, S xv, Ca xix, and Fe xxv ($Z=26$) are given in Table 1.

These He-like lines were first observed in laboratory for C, F, Mg, Al (see Edlén, 1947) and later in solar plasmas thanks to the Orbiting Solar Observatory (OSO), and rocket experiments (e.g., Fritz et al., 1967; Doschek and Meekins, 1970; Acton et al.,

	C V	N VI	O VII	Ne IX	Mg XI	Si XIII	S XV	Ca XIX	Fe XXV
w	40.2674 (0.3079)	28.7870 (0.4307)	21.6015 (0.5740)	13.4473 (0.9220)	9.1688 (1.3522)	6.6479 (1.8650)	5.0387 (2.4606)	3.1772 (3.9024)	1.8504 (6.7004)
x	40.7280 (0.3044)	29.0819 (0.4263)	21.8010 (0.5687)	13.5503 (0.9150)	9.2282 (1.3431)	6.6850 (1.8547)	5.0631 (2.4488)	3.1891 (3.8878)	1.8554 (6.6823)
y	40.7302 (0.3044)	29.0843 (0.4263)	21.8036 (0.5686)	13.5531 (0.9148)	9.2312 (1.3431)	6.6882 (1.8538)	5.0665 (2.4471)	3.1927 (3.8833)	1.8595 (6.6676)
z	41.4715 (0.2990)	29.5347 (0.4198)	22.0977 (0.5611)	13.6990 (0.9051)	9.3143 (1.3311)	6.7403 (1.8394)	5.1015 (2.4303)	3.2110 (3.8612)	1.8682 (6.6366)

Table 1 Wavelengths (in Å), and in parentheses energies (in keV) of the resonance (w), intercombination ($x + y$) et forbidden (z) lines for several He-like ions.

1972; Grineva et al., 1973). However the detection of a significant line coincident with the wavelength of a single photon transition from the metastable 3S_1 level to the ground level could not be understood from theory, because the metastable level was expected to decay only by two-photon emission. Gabriel and Jordan (1969a) strongly suggested that this line might correspond to some unknown photon transition. This was confirmed by a quantum-relativistic calculation of Griem (1969) who proved that indeed the 3S_1 level has a significant single-photon decay rate, so a line can be observed. Then Gabriel and Jordan (1969b) proposed that the relative intensities of these lines can be used for temperature and density diagnostics (see section 4) for solar plasma:

$$\mathcal{R} (n_e) \equiv \frac{z}{x + y} \quad \left(\text{or} \equiv \frac{F}{I} \right) \quad (1)$$

$$\mathcal{G} (T_e) \equiv \frac{z + (x + y)}{w} \quad \left(\text{or} \equiv \frac{F + I}{R} \right) \quad (2)$$

These diagnostics have first been widely used for solar spectra (e.g., Doschek and Meekins, 1970; Acton et al., 1972; McKenzie et al., 1980; Wolfson et al., 1983; Keenan et al., 1984; Doyle and Keenan, 1986) and for X-ray spectra of tokamak plasmas (e.g., Källne et al., 1983; Keenan et al., 1989).

It is now possible, thanks to the spectral resolution and the sensitivity of the current generation of X-ray satellites *Chandra* and *XMM-Newton*, to resolve the He-like ion lines and to use these diagnostics for extra-solar objects. Indeed, the He-like ion line ratios are valuable tools in the analysis of high-resolution spectra of a variety of plasmas such as:

- Collisional Ionization Equilibrium (CIE) plasmas or also called coronal plasmas: in such plasmas, ionization is due to electron-ion collisions and the atomic levels are populated mainly by electron impact. It is commonly assumed that CIE plasmas are optically thin to their own radiation, and that there is no external radiation field that affects the ionization balance. However, in some cases, these assumptions are not fulfilled as discussed in sections 3 and 4.
E.g., solar and stellar coronae (OB stars, late type stars, active stars, T Tauri, ...), cluster of galaxies, the hot intra-cluster medium, Galactic ridge and Galactic center X-ray emission, ...
- Recombination-dominated or Photo-Ionization Equilibrium (PIE) plasmas: in such plasmas, ionization is due to photons (ionizing radiation) and the atomic

levels are populated mainly by radiative recombination of H-like ions to He-like ions directly or by cascade from upper levels. These plasma are generally overionized relative to the local electronic temperature and have a much smaller electronic temperature compared to CIE plasmas. That is why collisional excitations out of the ground state are inefficient and excited levels are populated via radiative recombination. However, as we will see in section 3, photo-excitation can be a non-negligible process.

E.g., Active galactic nuclei, X-ray binaries, ...

- Out of equilibrium plasmas, or non-ionization equilibrium (NIE) plasmas: Some astrophysical plasmas depart from ionization equilibrium. This occurs when one or several physical conditions of the plasma suddenly change, such as the temperature (section 3.2), the density, or the photo-ionization radiation field.

E.g., Supernova remnants, solar and stellar flares, colliding winds in star clusters and X-ray binaries, cluster of galaxies, intra-cluster medium in merging galaxy clusters,

Since the pioneering work of Gabriel and Jordan (1969b), several works have been dedicated to the improvements of these diagnostics based on He-like line ions and their extension to other types of plasmas (photo-ionization equilibrium and non-ionization equilibrium): e.g., Mewe (1972), Blumenthal et al. (1972), Gabriel and Jordan (1973), Mewe and Schrijver (1975, 1978a,b,c), Acton and Brown (1978), Pradhan and Shull (1981), Bely-Dubau et al. (1982), Pradhan (1982, 1985), Keenan et al. (1984), Swartz and Sulkanen (1993), Liedahl (1999), Porquet and Dubau (2000); Porquet et al. (2001a), Bautista and Kallman (2000), Porter and Ferland (2007), and Smith et al. (2009).

In the present paper, we review why and how the relative intensities of the He-like ion lines can be used for plasma diagnostics. We also present several observational results based on these diagnostics for different types of plasmas. Since a large number of papers dealing with He-like ions has been published, this review cannot be exhaustive.

The outline of this paper is as follows. First, we give a brief overview of atomic structure and a few basic processes that play an important role for the population of the upper level of the $n=2$ shell in He-like ions (sect. 2). Section 3 concerns diagnostics of the different ionization processes: CIE and PIE plasmas (sect. 3.1), NIE plasmas (sect. 3.2), and charge-transfer (sect. 3.3). Section 4 is dedicated to electronic temperature (sect. 4.1) and electronic density (sect. 4.2) diagnostics. Section 5 presents the possible diagnostics based on the satellite lines. In the last section, we conclude and bring some possible perspectives for the future of plasma diagnostics based on He-like ions and their satellite lines thanks to the next generation of X-ray satellites, such as *Astro-H* and *IXO*.

2 Atomic processes and atomic data

Here we briefly introduce the main atomic processes that lead to the formation of He-like ion lines, as well as the impacts of atomic data, atomic model and spectral resolution on the calculation of the He-like line ratios. For more details about X-ray spectroscopy and atomic processes, see e.g., the very nice reviews from Liedahl (1999), Mewe (1999), Paerels and Kahn (2003), Kahn (2005) and Kaastra et al. (2008).

2.1 Main atomic processes

As illustrated on the Grotrian diagram reported in Fig. 1 (see also Fig. 1 in Mewe and Schrijver 1978a), the atomic levels of the He-like ions can be populated and depopulated by several atomic processes.

Collisional excitation inside He-like ions

In most plasmas, collisional excitations are mainly due to (projectile) electrons, however collisional excitation by protons and α -particles can be important in some cases (see below).

Electron collisional excitations from the $1s^2\ ^1S_0$ (ground) level to excited levels ($n=2$ and higher) require a large projectile energy to open the $1s^2$ shell. They become efficient as temperature increases and favors the population of singlet levels, such as 1P_1 level (hence the resonance w line). The excitation process of singlet excited levels from the singlet ground state does not require a change of the target spin. On the contrary, excitation of triplet levels is only possible by exchange of the projectile electron with one of the target electrons. As projectile energy increases, the exchange process becomes less efficient than the direct process, i.e., the non-exchange process. For highly ionized He-like ions, the spin-orbit interaction becomes important : spin-orbit interaction between singlet and triplet levels, for example $1s2p\ ^3P_1$ mixed with $1s2p\ ^1P_1$. It is responsible for the similar temperature behavior for 1P_1 and 3P_1 excitations. At high temperature, radiative cascade contributions from $n > 2$ levels populate the $n \geq 2$ levels, cascades remaining inside singlet levels or triplet levels respectively. Due to the small radiative probabilities from the $n=2$ triplet level to the singlet ground level, this favors the populations of triplet levels, namely $^3P_{0,1,2}$ and 3S_1 , compared to the singlet levels which can decay more directly to the ground level. At low temperature, the contribution of the auto-ionizing resonances to the electron scattering cross-sections enhances the forbidden z (and in a smaller part the intercombination ones, x and y) transition far more than the resonance transition (Pradhan and Shull, 1981).

Excitations inside the $n = 2$ shell should be taken into account even for low temperature plasmas, i.e., for photo-ionized plasmas. First, the metastable 3S_1 level can be depopulated to the $^3P_{0,1,2}$ levels when the density is high enough, i.e., above the so-called critical density (that depends on the He-like ions, see section 4.2). At much higher density, the $1s2s\ ^1S_0$ level (upper level of the 2-photon transition) can be depopulated to $1s2p\ ^1P_1$, thereby increasing the intensity of the resonance line (Gabriel, 1972).

The calculations of proton impact excitation rates by Blaha (1971) show that their contributions (and in a smaller part those of α -particles) can be non-negligible for high- Z (i.e., >14) ions at very high temperature (Mewe and Schrijver, 1978a). However, new

calculations of these proton excitation rates are required (Dubau et al., in preparation).

Recombinations from H-like ions to He-like ions

Recombinations from H-like ions to He-like ions can be due to radiative recombination or dielectronic recombination. Radiative recombination is highly efficient at low temperature (few eV) such as in photo-ionized plasmas, and favors the populations of the triplet levels, due to their higher statistical weight compared to singlet level. On the contrary, dielectronic recombination is efficient for high temperature plasmas, but it also favors the triplet levels. It is negligible in the low temperature range (i.e., photo-ionized plasmas). Hence, both recombination processes lead to an intense forbidden or intercombination lines (depending on the density, see section 4.2) compared to the resonance line.

Inner-shell ionization of Li-like ions

Inner-shell ionization of Li-like ions can significantly contribute to the formation of the forbidden line of He-like ions, hence increasing the value of the \mathcal{R} ratio at the low density limit and the value of the \mathcal{G} ratio (e.g., Doschek and Meekins, 1970; Gabriel, 1972; Mewe and Schrijver, 1975, 1978a; Oelgoetz and Pradhan, 2004). For this process to have an impact on the intensity of the forbidden He-like ions, both the relative abundance of Li-like to He-like, $N(\text{Li-like})/N(\text{He-like})$, and the ionization coefficient rate must be large. This latter condition is reached at high temperature. In collisional ionization equilibrium plasmas and close to the temperature of maximum formation of He-like ions, both conditions are not fulfilled since the relative abundance of Li-like ions is very small. A high abundance of Li-like ions and a high electronic temperature can occur in transient plasmas such as a in supernova remnants and during solar/stellar flares (section 3.2), and this process is important especially for high- Z ions.

Other atomic and physical processes

Other atomic processes should be considered in some cases such as photo-excitation (section 4.2) or charge exchange (section 3.3). For very high densities, not considered here, several atomic processes have to be taken into account (e.g., Bautista and Kallman, 2000). In addition, resonance line scattering and optical depth might have an impact on the line ratios (section 3.1).

2.2 Importance of the accuracy of the atomic model and atomic data

As shown by several authors, to perform line ratio calculations it is of importance to use a good atomic model with accurate atomic data (e.g., Mewe and Schrijver, 1978a; Pradhan and Shull, 1981; Porquet and Dubau, 2000; Porquet et al., 2001a; Bautista and Kallman, 2000; Smith et al., 2001, 2009; Porter and Ferland, 2007).

It is not possible to use a LS model of He-like states to simulate the intensities of the resonance, intercombination and forbidden lines even for low charge He-like ions. Nevertheless some fine-structure data can be converted from LS data, particularly collisional data due to the non-relativistic nature of the main electron-electron interaction, $1/r_{ij}$. Be aware, however it can not be used as a general rule because relativistic effects increase rapidly as the nuclear charge increases. A second point concerns the number of He-like levels included in the model, and maybe H-like and Li-like levels

as well. The $n = 2$ triplet levels, 3S_1 , $^3P_{0,1,2}$ being very sensitive to recombination from H-like ions, the model must include high $n > 2$ levels cascading to $n = 2$ levels, even at low temperature. As temperature increases, radiative cascades contribution from collisional excitation of high $n > 2$ levels can have also a significant influence on the populations of the $n = 2$ levels (e.g., Porquet and Dubau, 2000; Smith et al., 2009). Electron ionization from Li-like ions is also possible and has a direct influence on the forbidden line intensity. Besides, proton and α -particle excitations might play a role on the density diagnostic for high- Z He-like ions. A reliable simulation therefore requires collecting first a huge amount of accurate atomic data related to $n = 2$ and also to $n > 2$, up to $n = 5$, or may be $n=10$. Papers giving all these data with great accuracy do not exist. Some papers contain apparently very accurate data for electron excitation but for only very few transitions. Further papers assert that the preceding calculations are not complete because they do not contain some important effects, such as radiation damping of resonances, which invalidate their accuracy. On the other hand, some authors give apparently less accurate data but including these effects. To illustrate this last point, we mention the impressive work of Sampson et al. (1983), for electron collisional excitation of He-like excited levels for $n = 1$ and $n = 2$ up to $n = 5$, for $4 \leq Z \leq 74$. It is a Coulomb-Born-Exchange (CBE) calculation between fine-structure levels, apparently not very accurate. In particular, auto-ionizing resonances are not included. But they were inserted, including also radiation damping, in a following work by Zhang and Sampson (1987). Indeed, auto-ionizing resonances have to be taken into account for a good calculation of collisional excitation rates (e.g., Pradhan and Shull, 1981; Smith et al., 2009). But how to include them correctly ? There exists two different approaches either implicitly or explicitly. CBE, already mentioned, or Distorted Wave (DW) data do not include at all auto-ionizing resonances but it is possible to include them explicitly afterward. Whereas in Close-Coupling approximations, such as R-matrix (non-relativistic, Breit-Pauli or Dirac formalisms), they are implicitly included. These later approximations are therefore apparently better. But these resonance effects can be strong and, sometimes they are strongly overestimated because auto-ionizing resonances can also decay by radiative transitions not included in the approximations, the so-called radiation damping effect. The radiation damping is also responsible for Dielectronic Recombination, included in the model but as a recombination process (see a later section). One must therefore takes care not to include twice the same process, i.e., to separate the two decays of resonance either as excitation or as recombination. Many different methods have been proposed to overcome this problem of radiation damping in close-coupling calculations, (e.g., Zhang and Pradhan, 1995). They can give different results. What are the best ? The comparison between all these atomic data obtained by different methods is very interesting but beyond the scope of this review.

Experimental measurements of the atomic data and/or line ratio of He-like ions in laboratory devices, such as tokamak, EBIT (e.g., Källne et al., 1983; Keenan et al., 1989; Beiersdorfer et al., 1992; Wargelin et al., 2008; Beiersdorfer et al., 2009; Brown et al., 2009) could be of great importance to resolve some discrepancies between theoretical calculations and observations (e.g., Ness et al., 2003b; Testa et al., 2004a; Chen et al., 2006; Smith et al., 2009). As a summary on this point, the most important is first to have a good atomic model containing the best data.

2.3 Impact of the spectral resolution

Blending of the He-like lines with satellite lines (defined in section 5) depends on the resolution of the observed spectra. Therefore, the calculations of the line ratio have to take into account contributions from unresolved satellite lines, especially for high- Z ions (see e.g., Porquet et al., 2001a; Sylwester et al., 2008). At low and moderate spectral resolutions all satellite lines are unresolved. In the near future higher spectral resolution will be obtained thanks to X-ray calorimeters and gratings (aboard e.g., Astro-H and IXO) at high energies and some $n=2-3$ satellites lines will be resolved for high- Z ions, and can be used to probe plasma properties (see section 5). However $n > 3$ satellite lines will not be resolved and the \mathcal{G} and \mathcal{R} ratio calculations must account for their contributions. Additionally, possible contamination could be due to other elements such as Fe XIX lines with the intercombination line of Ne IX lines for high enough temperature (McKenzie et al., 1980; McKenzie, 1985; Wolfson et al., 1983; Ness et al., 2003b).

3 Ionization process diagnostic

3.1 Collisional-dominated versus photo-ionized plasmas

The relative intensity of the three lines can be used to discriminate between a collisional-dominated plasma (CIE) and a photo-ionized (recombination-dominated) plasma (PIE). At high electronic temperature, as in collisional plasma, the collisional excitation process is efficient. Therefore this favors the population of the 1P_1 level, hence the resonance line w is intense. The value of the \mathcal{G} ratio is around 1 (see section 4.1). While at low electronic temperature, as in photo-ionized plasma, recombination is the dominant process. Recombination favors the population of the $^3P_{0,1,2}$ and 3S_1 levels, hence the forbidden and/or the intercombination lines are intense. The value of the \mathcal{G} ratio is equal or greater to 4. To illustrate this effect, the relative intensities of the O VII triplet lines for collisional and photo-ionized plasmas are shown in Fig. 2. This diagnostic has been used for active galactic nuclei (e.g., NGC 4051: Collinge et al. 2001; NGC 4593: McKernan et al. 2003; NGC 4151: Schurch et al. 2004) and X-ray binaries (e.g., EXO 0748-67: Cottam et al. 2001; Jimenez-Garate et al. 2003) where \mathcal{G} greater than or similar to 4 were found, confirming the photo-ionization as the main ionizing process in these objects. However this diagnostic based on the value of the \mathcal{G} ratio to disentangle between a collisional plasma and a photo-ionized plasma should be used with caution when *resonance line scattering* and optical depth are not negligible.

At non-negligible optical depth ($\tau \sim 1$), resonance line scattering occurs: a photon (from a continuum or a line) at a certain wavelength can be absorbed by ions, and then re-emitted due to a transition at the same wavelength but generally in a different direction. The scattered resonant photons emerge into the direction of the lowest optical depth, then decreasing the observed value of \mathcal{G} , while in the direction of the highest optical depth, the observed value of \mathcal{G} is raised. Therefore the total photon intensity integrated over all directions remains unchanged but the photon distribution with respect to a given direction is altered. Thus its effects depends on the geometry of the region being observed. One should notice that in case of a spherical source resonant line scattering does not affect the emergent spectrum. Resonance line scattering first occurs in transition with large oscillator strengths, such as the so-called resonance lines. From C V to Si XIII, in case of a collisional plasma, the resonance line becomes

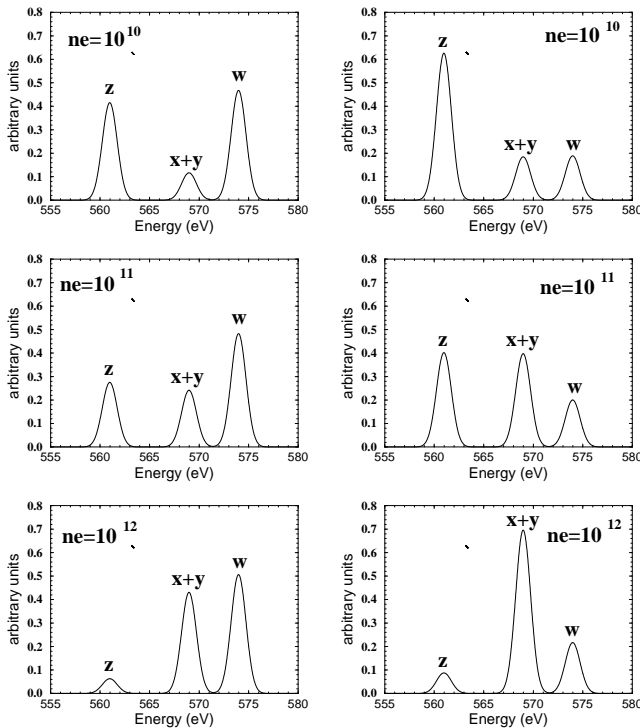


Fig. 2 Comparison of theoretical spectra of the O VII triplet lines at the spectral resolution of the RGS aboard *XMM-Newton*. z , $x + y$ and w mark the forbidden, intercombination and resonance lines, respectively. Left and right panels show collisional-dominated and photo-ionized (recombination-dominated) plasmas, respectively. The three values of electronic density corresponds to the density range where the relative intensities of z and $x + y$ line vary. The intensities are normalized so as the sum of the lines to be equal to unity. Figure from Porquet and Dubau (2000). Courtesy of Astronomy and Astrophysics.

sensitive to resonant lines scattering for $N_{\text{H}} \sim 10^{21} - 10^{23} \text{ cm}^{-2}$, while the intercombination and forbidden lines are only sensitive for much higher column density: $N_{\text{H}} \sim 10^{25} - 10^{26} \text{ cm}^{-2}$, and $N_{\text{H}} \sim 10^{30} - 10^{31} \text{ cm}^{-2}$, respectively (Porquet et al., 2001a). Depending of the geometry of the plasma (and of the radiation source if spatially distinct), the apparent intensity of the resonance line can be enhanced, decreasing the observed \mathcal{G} ratio value. Thus a higher temperature plasma could erroneously be inferred. In case of a photo-ionization, a collisional plasma could be mimicked by an apparent low value of \mathcal{G} (e.g., Schulz et al., 2002). This is nicely illustrated by Wojdowski et al. (2003), who found that in the case of the high-mass X-ray binary, Centaurus X-3, the \mathcal{G} ratio outside the eclipses is consistent with the value expected in photo-ionized plasma (or more correctly “pure” recombination plasma); while during the eclipse the \mathcal{G} ratio is much lower and consistent with the value expected in case of a collisional plasma. However, they explained this apparent change of the \mathcal{G} ratio as due to the effects of resonance line scattering (in addition to the recombination process). Indeed, outside the eclipse both the absorption and the emission component of the resonance line scattering process are observed, then “cancel out” the apparent contribution of

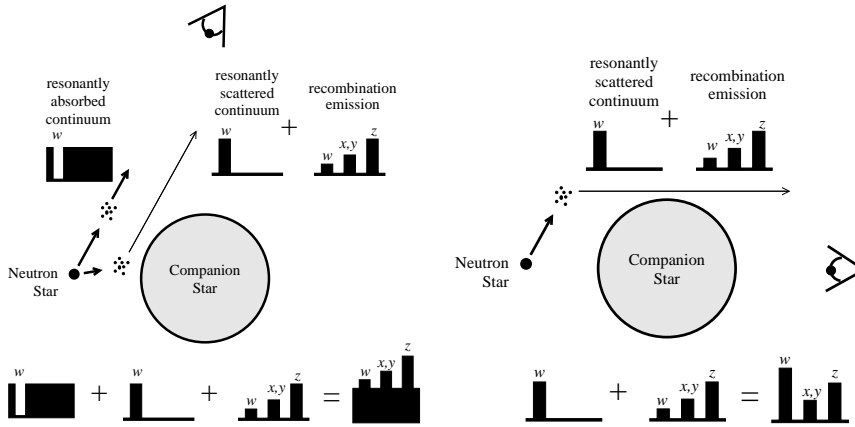


Fig. 3 Schemes illustrating the impact of resonance line scattering contribution (absorption and/or emission) on the observed \mathcal{G} ratio values for the high-mass X-ray binary, Centaurus X-3. Left and right panels show the configuration outside and during the eclipse. Figures from Wojdowski et al. (2003). Reproduced by permission of the AAS.

this additional process (see fig. 3, left panel); while during the eclipse only the emission component of the resonance line scattering is observed, increasing the intensity of the resonance line, and then decreasing the value of the observed \mathcal{G} ratio (see fig. 3, right panel), mimicking a hot plasma. This is the same effect as observed in obscured active galactic nuclei where only the emission part of the resonance line scattering is observed, then leading in some cases to a \mathcal{G} ratio smaller than expected for a “pure” photo-ionized plasma (e.g., NGC 1068: Kinkhabwala et al. 2002, Brinkman et al. 2002; Guainazzi and Bianchi 2007). For more details about resonance line scattering, optical depth and column density impacts, see also Schmelz et al. (1997) Wood and Raymond (2000), Porquet et al. (2001a, 2002), Ness et al. (2003a), Testa et al. (2004b, 2007), Bianchi et al. (2005), Waldron and Cassinelli (2007), Leutenegger et al. (2007), Porter and Ferland (2007), Argiroffi et al. (2009), and Churazov et al. 2010 (this volume).

In conclusion, in case of non-negligible resonance line scattering and optical depth, additional plasma diagnostics should be used to discriminate between a collisional plasma and a photo-ionized one, such as those based on the width measurement of the recombination recombination continuum (RRC) features (Liedahl and Paerels, 1996; Liedahl, 1999), and on the line ratios of Fe L lines (Liedahl et al., 1990; Kallman et al., 1996).

3.2 Non-ionization equilibrium plasmas

We now consider non ionization equilibrium (NIE) that occurs when the physical conditions of the source, such as the temperature, suddenly change (transient plasmas). In cases where the time-scale of temperature fluctuation is shorter than the time-scale of ionization equilibrium, the assumptions of ionization equilibrium is not fulfilled. Indeed, it takes a finite time for the plasma to respond to the temperature change, with different atomic process time-scales: for example at high temperature electron excitation time-scales are shorter than electron ionization time-scales that are shorter than recombination time-scales. Since, both ionization and recombination rates depends on the electronic density, time to fulfill ionization equilibrium depends on its value. Typically hot plasmas are out of equilibrium for $n_e t \lesssim 10^{10} - 10^{13} \text{ cm}^{-3} \text{ s}$ (e.g., Smith and Hughes 2010). Therefore, the smaller the density is, the longer plasma is in non-ionization equilibrium. The variations with time of the line intensities of the He-like ions indicates the succession through the consecutive ionization stages and the impact of the different population level processes (e.g., Mewe and Schrijver, 1975, 1978b; Acton and Brown, 1978; Liedahl, 1999; Oelgoetz and Pradhan, 2004). For example, an abrupt increase of the temperature can occur during solar/stellar flares or after a shock in a supernova remnant. The plasma is initially ionizing, and the state of ionization is lower than the equilibrium value at the local temperature. As illustrated in Fig. 4, the ionic fractions calculated for a NIE plasma differ drastically from that found in CIE plasma.

At the early stage of the temperature increase, a significant abundance of Li-like ions can exist at high temperature together with He-like ions, contrary to that found

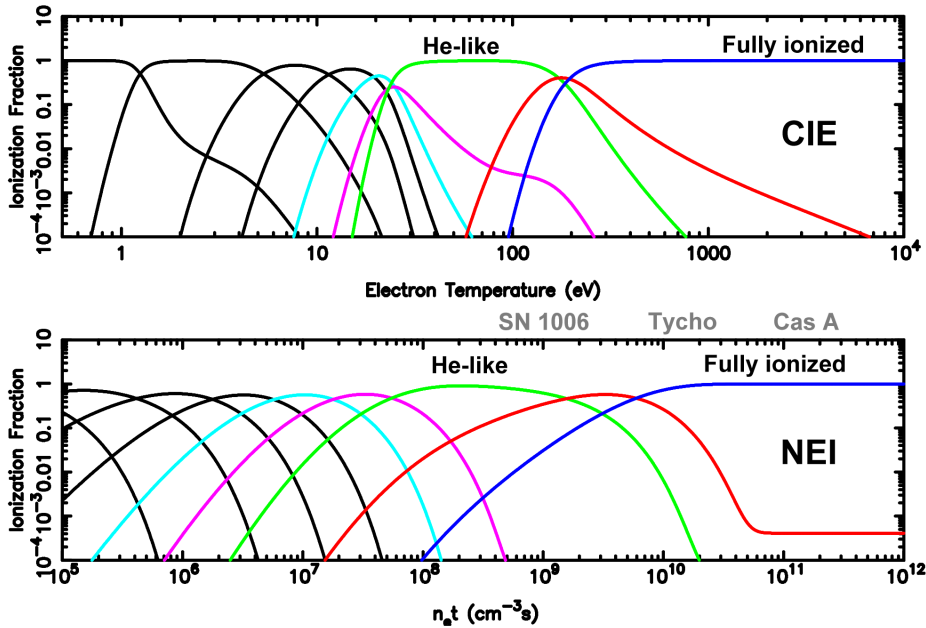


Fig. 4 O VII ionic fraction abundances for a collisional plasma (CIE), and a non-ionization equilibrium plasma (NIE) for a fixed electronic temperature of 1.5 keV. Figure from Vink (2006). Courtesy of ESA publication.

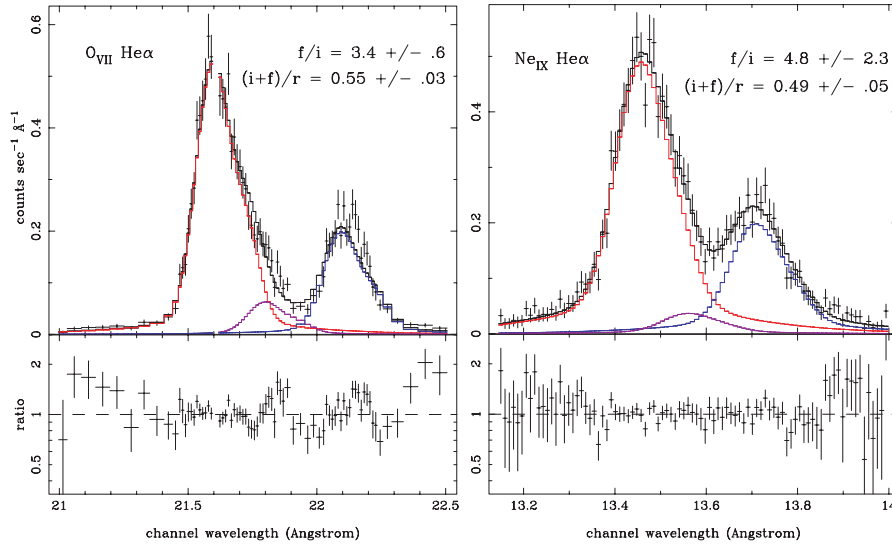


Fig. 5 O VII and Ne IX lines observed from the supernova remnants 1E 0102.2-7219 . The inferred values of \mathcal{R} and \mathcal{G} ratios are reported. The small values of the \mathcal{G} ratio indicate that the plasma is ionizing. Figures from Rasmussen et al. (2001). Courtesy of Astronomy & Astrophysics.

found in CIE plasma. Therefore, inner-shell ionization of Li-like ions ($1s^2 2s$) can be important, especially for high- Z ions, and then favoring the population of the 3S_1 level of the He-like ions (e.g., Mewe and Schrijver, 1975, 1978b; Mewe et al., 2003b, see also section 2). Hence in such case, the \mathcal{G} ratio can be higher than for a CIE plasma of the same temperature. We would like to notice that in such case Li-like satellites lines should be observed too, especially for high- Z ions (see section 5). Such conditions can be found at the beginning of a solar/stellar flares (see e.g., Mewe and Schrijver, 1975, 1978b) or behind the shock front in supernova remnants (e.g, SN 1006: Vink et al. 2003). One should notice that in case of efficient inner-shell ionization of Li-like ions, the value of the ratio \mathcal{R} is enhanced as well compared to that found for ionization equilibrium plasmas.

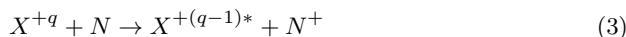
At higher temperature when the abundance of Li-like ions becomes negligible and the plasma is still ionizing, recombination can be partly or totally quenched, especially when the ionic fraction of H-like ions is negligible. In such case the \mathcal{G} ratio is much smaller than that found for a CIE plasma at the same temperature. The temperatures inferred from the \mathcal{G} ratio correspond to temperatures well above the maximum emission temperature found for a collisional equilibrium plasma. Such low \mathcal{G} values have been found in several supernova remnants (Puppis A: Winkler et al. 1981; Cygnus Loop: Vedder et al. 1986; 1E 0102.2-7219: Rasmussen et al. 2001; Flanagan et al. 2004; G292.0+1.8: Vink et al. 2004). For illustration, the triplet ratios for O VII and Ne IX observed for the supernova remnant 1E 0102.2-7219 are shown in Fig. 5.

In a recombining (or cooling) plasma the ratio of H-like to He-like ions may be much higher than that corresponding to the local electronic temperature. Therefore, the recombination is enhanced and then would preferentially populate the triplet levels. And depending of the density, either the intensity of the forbidden line or the intercombination line(s) is boosted compared to a CIE plasma of the same temperature. Such conditions may occur during a decay phase of the temperature during solar/stellar flares (e.g., Doschek and Meekins, 1970; Mewe and Schrijver, 1978b) or during the expansion phase of supernova remnants.

In conclusion, the relative intensities of the $1s\ 2p-1s^2$ He-like transitions, from C V to Fe XXV, could in principle provide a powerful test of departure from ionization equilibrium, i.e., heating/cooling stage in transient plasmas. Complementary diagnostics can be used likewise to assess departure from ionization equilibrium such as $1s\ n p-1s\ 2p$ ($n > 2$) ratios, satellite lines (see section 5), and Fe L lines.

3.3 Charge exchange/transfer

X-ray lines can also be produced by transfer/exchange collisions. When a neutral atom/molecule (N ; e.g., H, H₂, N₂, CH₄, H₂O, CO, CO₂) collides with a highly charged ions (X^{+q} ; e.g., H-like ions), one or more electron from the neutral atom/molecule is transferred to the ions (eq. 3). The recombining ion is usually in an excited state ($X^{+(q-1)*}$; e.g., He-like ions) and will be stabilized by radiative cascade (eq. 4).



This process has been proposed first proposed by Cravens (1997) to explain the unexpected extreme ultraviolet and soft X-ray emission from the comet Hyakutake in 1996 brought to light by ROSAT (Lisse et al., 1996). The brightest lines observed in cometary spectra are the He-like transitions of O VII, produced by the charge exchange of solar wind H-like O VIII ions with neutral targets (Bhardwaj et al., 2007). This process has also been proposed to explain partly or totally the soft X-ray emission of several astrophysical objects: comets, atmospheres of planets (e.g., Mars halo), Jupiter's aurora, heliosphere, terrestrial magneto-sheath, north polar spur, stellar winds, supernova remnants, and intra-cluster gas (e.g., Cravens 2000; Dennerl et al. 1997, 2006; Krasnopolsky et al. 2004; Bhardwaj et al. 2007; Branduardi-Raymont et al. 2007; Lallement 2004; Fujimoto et al. 2007; Koutroumpa et al. 2007). Charge exchange cross-sections at solar wind ion energies are quite large, typically about 10^5 times larger than those for electron collisional excitation. Therefore charge exchange process can be very efficient even for a small abundance of neutral hydrogen. Recent calculations and experiments show that the forbidden line is the brightest line of the He-like ions (e.g., Beiersdorfer et al. 2003, 2005; Kharchenko et al. 2003; Pepino et al. 2004; Wargelin et al. 2005; Bodewits et al. 2007; Brown et al. 2009). This is due to the fact that three-quarter of the captures occur into triplet states and radiate preferentially by allowed cascade transition into the 3P levels (that can partly – or totally for the 3P_0 level – decay to the 3S_1 level) and the 3S_1 metastable level. Therefore even in case of moderate spectral resolution of shift of the energy centroid of the triplet lines towards that of the forbidden lines (or that of the intercombination line in case of high density,

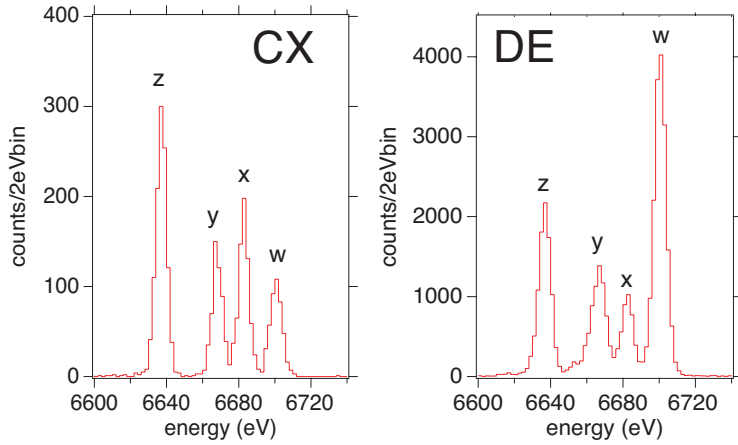


Fig. 6 Experimental spectra of Fe xxv obtained with the LLNL SuperEBIT facility for charge exchange (CX) between Fe xxvi and N₂ (left panel) and for direct electron impact excitation (right panel). Figure from Brown et al. (2009). Courtesy of Journal of Physics Conference Series.

see section 4.1) could be the signature of charge transfer (or photo-ionized plasma as discussed in section 3.1). As an illustration, Figure 6 shows the experimental spectrum of Fe xxv obtained with the LLNL SuperEBIT facility for both charge exchange and electron-impact excitation (Brown et al., 2009).

In case of O VII, values of the \mathcal{G} ratio have been estimated to about 12.5, 6.7 and 4.0 by Kharchenko et al. (2003), Pepino et al. (2004), Bodewits et al. (2007), respectively. The value of the line ratios depend on the nature of ions (atomic number and ionization state) and of the neutral target (i.e, H, He, ...) and its velocity. Therefore high-spectral resolution coupled with high S/N spectrum should be able to distinguish between capture from Hydrogen or from Helium.

Recently, Mars was observed with the RGS aboard XMM-Newton, and the O VII triplet was resolved (Dennerl et al., 2006). The spectrum of Mars halo shows the forbidden line is the dominant line of the triplet, with no evidence of the presence of the intercombination lines, and only an indication for the presence of the resonance line (see fig. 7). This is consistent with the signature of charge exchange as the source of the X-ray emission. The \mathcal{G} values derived from the Mars spectra are $\mathcal{G} \sim 6$ for $|y| \leq 50''$. This ratio value is consistent with the above mentioned predicted value derived for charge exchange. However, as mentioned by Dennerl et al. (2006), the exact value of the \mathcal{G} ratio is highly uncertain, because only the forbidden line is statistically significant.

For a detail review about the charge transfer/exchange process and its astrophysical applications, see Dennerl et al. (2010, this volume) and references therein.

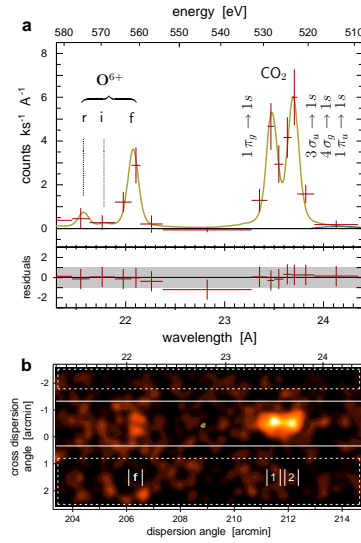


Fig. 7 XMM-Newton/RGS 1 spectrum of Mars and its halo at cross dispersion distances $|y| \leq 50''$ from the center of Mars, showing the O VII triplet (Dennerl et al., 2006). Figure from Dennerl (2009). Courtesy of Advances in Geosciences.

4 Electronic temperature and density diagnostics

4.1 Electronic temperature diagnostic

In the case of a collisional plasma, such as a stellar corona, the electronic temperature can be determined using the value of the \mathcal{G} ($\equiv (z + x + y)/w$ or also $\equiv (F + I)/R$) ratio (e.g., Gabriel and Jordan, 1969b; Mewe and Schrijver, 1978a; Porquet and Dubau, 2000). Indeed the collisional excitation rates do not have the same dependence on temperature for the three lines: the intensity of the w line increases more rapidly with the temperature than those of the z and x lines (see section 2). Therefore, the \mathcal{G} ratio decreases when the temperature increases. As an illustration, the left panel of figure 8 reports the \mathcal{G} ratio versus the temperature for O VII.

Different temperature ranges can be probed since each ion has a specific temperature where the line emissivity is maximum that increases with the charge of the ion (Z). To illustrate this point, we report in Fig. 9 the range of electronic temperature where the emissivity for the resonance line is greater than 10% of the maximum, computed with the CHIANTI database version 6.0.1 (Dere et al., 1997, 2009) using the CIE calculations of Bryans et al. (2009). When the plasma temperature increases low- Z elements are easily totally ionized, so only He-like ions from high- Z elements are present. In the most favorable case where the plasma temperature is about 2 MK, up to five He-like ions (from N VI to Si XIII) can be present simultaneously in the plasma. However in case of resonance line scattering or large optical depth, the intensity of the resonance line can be enhanced or reduced (see section 3.1), therefore the determination of the temperature can be biased.

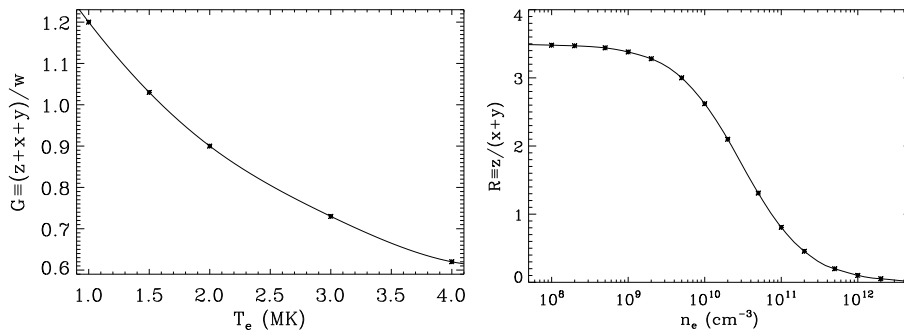


Fig. 8 Electronic temperature (T_e) and density (n_e) plasma diagnostics for the He-like O VII ion. *Left panel:* $\mathcal{G} \equiv (z+x+y)/w$ versus T_e for $n_e=10^{10} \text{ cm}^{-3}$. *Right panel:* $\mathcal{R} \equiv z/(x+y)$ versus n_e for $T_e=10^6 \text{ K}$. Calculations are taken from Porquet et al. (2001a).

Moreover, the \mathcal{G} ratio is independent of the density when the density is low enough to prevent:

- the depopulation of the $1s2s\ ^1S_1$ level to the $1s2p\ ^1P_1$ level (see section 2);
- the depopulation of the $n=2$ level by collisional ionization;
- the collisional transfer from triplet to singlet term.

As mentioned in section 2, the contributions of blended satellite lines (that depend upon spectral resolution) must be taken into account in the calculations of the intensity of the He-like lines (e.g., Porquet et al., 2001a; Sylwester et al., 2008). In the near future, some satellite lines will be resolved for extra-solar objects and their intensity ratio over the resonance line will provide a useful temperature diagnostic (see section 5). In addition, the relative intensity of the $1s^2-1snp$ (with $n > 2$) lines to the $1s^2-1s2p\ ^1P_1$ resonance line can be used for temperature diagnostics (Gabriel and Jordan, 1973; Keenan et al., 1985).

The ratio of the resonance lines of H-like/He-like ions is widely used as well for temperature diagnostics, since this ratio increases rapidly with the temperature. Contrary to the \mathcal{G} ratio that is based on the line ratio of only one ion, the H-like/He-like ratio gives the temperature where both He-like ions and the more highly ionized H-like ions are formed. When using this ratio, one assumes that the two ions are formed in the same region and in the same volume, which may not be the case. Moreover, this ratio depends on the accuracy of ion fraction calculations, and any departures from ionization equilibrium will lead to a misleading estimate of the temperature. As also mentioned for the \mathcal{G} ratio, some line blending, resonance line scattering or optical depth effects could occur and should then be taken into account.

4.2 Electronic density diagnostic

4.2.1 In the case of negligible UV radiation field

The density diagnostic is based on the \mathcal{R} ratio ($\equiv z/(x+y)$ or $\equiv F/I$). In the low-density limit, both upper levels of the forbidden transition and of the intercombination transitions (3S_1 level and $^3P_{0,1,2}$ levels, respectively) decay radiatively. The relative intensities of these lines are then independent of the density. This is the so-called “low density limit” (\mathcal{R}_0). The value of \mathcal{R}_0 decreases with the atomic weight of the ions (e.g., Porquet et al. 2001a; Bautista and Kallman 2000). When the electronic density, n_e , increases from the low-density limit, and reaches the critical density¹, the collisional excitation starts to depopulate the upper level of the forbidden line to the upper levels of the intercombination lines. Consequently, the intensity of the *forbidden* line decreases while those of the *intercombination* lines increase, thus implying a reduction of the ratio \mathcal{R} over approximately two or three decades of density. The right panel of Fig. 8 shows the intensity ratio of the forbidden line over the intercombination line for O VII versus the electronic density (see also Fig. 2 for illustration). As explained previously, in the low-density regime, \mathcal{R}_0 is insensitive to the density value, and here $z \gg x+y$ (with the value of \mathcal{R}_0 depending upon the He-like ion considered as mentioned above; for iron \mathcal{R}_0 is about unity so $z \sim x+y$). In this case, we can infer an *upper limit* for the density value (e.g., \sim a few 10^9 cm^{-3} for O VII). For n_e greater than the critical density, the intercombination line flux increases while the forbidden line flux decreases. Therefore the \mathcal{R} ratio is very sensitive to the electronic density, and one can infer a precise value of n_e . For example, for the O VII ion reported in Fig. 8, a ratio equal to 2 corresponds to a density value of $3 \times 10^{10} \text{ cm}^{-3}$. When $(x+y) \gg z$ (i.e., z tends to zero), one can infer only a lower limit for the density value, e.g., about 10^{12} cm^{-3} for O VII. We report in Fig. 9 the typical ranges of plasma density where He-like triplets, from C V to Si XIII ions, are *very* sensitive to the density. These diagnostics based on He-like ions can probe a large density range from a few 10^7 cm^{-3} (C V) to a few 10^{17} cm^{-3} (Fe XXV). For a CIE (or PIE) plasma, high- Z ions measure high density and high temperature (or ionization parameter), while low- Z ions measure low density and low temperature (or ionization parameter) plasmas.

We would like to notice that the value of \mathcal{R}_0 is sensitive to the temperature (Pradhan, 1982; Porquet and Dubau, 2000; Smith et al., 2009). Indeed, the forbidden line can be enhanced compared to the intercombination lines (until n_e is lower than the critical density):

- by radiative cascade following collisional excitations to high n ($n \geq 3$) levels, at high temperature (section 2).
- by inner-shell ionization of Li-like ions when both the abundance of Li-like ions and the corresponding ionization rate are high (at high temperature). This can occur in NIE plasmas (see sections 2 and 3.2).
- by the resonance contribution of auto-ionizing resonances to the electron scattering cross-sections at low temperature (section 2).

¹ The critical density n_{crit} is the value of density above which collisional excitation from the 3S_1 level to the $^3P_{0,1,2}$ begins to dominate the radiative decay from the metastable 3S_1 level to the ground level. In some works, the critical density is defined as the density where \mathcal{R} is about $\mathcal{R}_0/2$ (e.g., Güdel and Nazé, 2009).

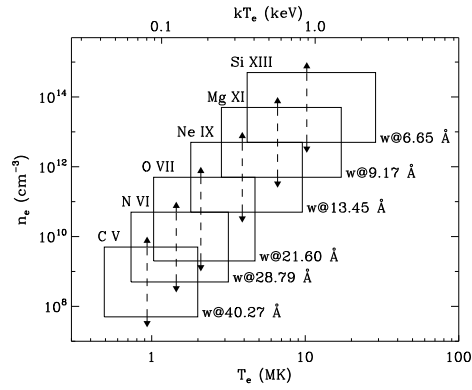


Fig. 9 Domain of electronic density and temperature where the He-like triplet diagnostics (from C V to Si XIII) can be used in case of collisional ionization equilibrium (CIE). The box width gives the range of electronic temperature where the emissivity for the resonance line is greater than 10% of the maximum, computed with the CHIANTI database version 6.0.1 (Dere et al., 1997, 2009) using the CIE calculations of Bryans et al. (2009). The dashed lines mark the electronic temperature where the maximum of the emissivity for the resonance line is achieved. The box height reports the density ranges of the \mathcal{R} ratio diagnostic, where a constrained value of the electronic density can be obtained. Below and above the boxes, only an upper limit and a lower limit of the electronic density can be obtained, respectively. The wavelengths of the resonance lines are reported.

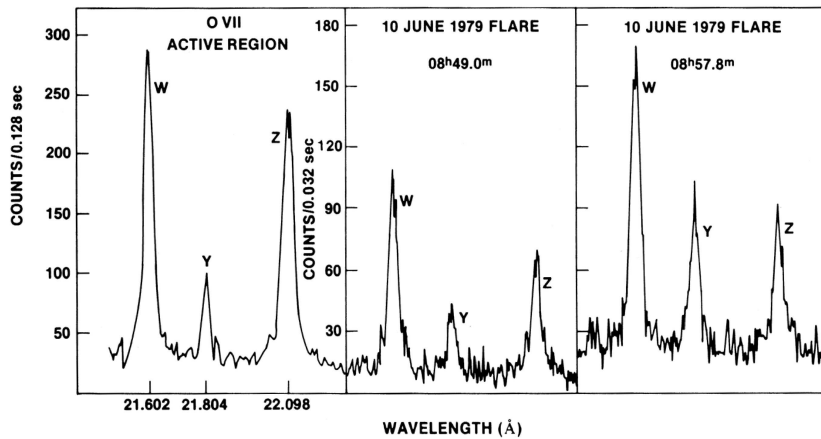


Fig. 10 The O VII triplet obtained from the Sun (SOLEX spectrometer experiment on the P78-1 spacecraft) for an active region and flares. Figure from Doschek (1983). Courtesy of Solar Physics.

As mentioned in section 2, the contributions of blended satellite lines (that depend upon spectral resolution) must be taken into account in the calculations of the intensity of the He-like lines, and hence for \mathcal{R} ratio calculations (e.g., Porquet et al., 2001a).

This density diagnostic has already been widely used in various type of astrophysical objects, such as solar and stellar coronae, active galactic nuclei, and X-ray binaries.

In case of the Sun, the \mathcal{R} ratio for low- Z ions (e.g., O VII, Ne IX, and Mg XI) show that the density for non-flaring active regions is about 10^9 cm^{-3} , while dur-

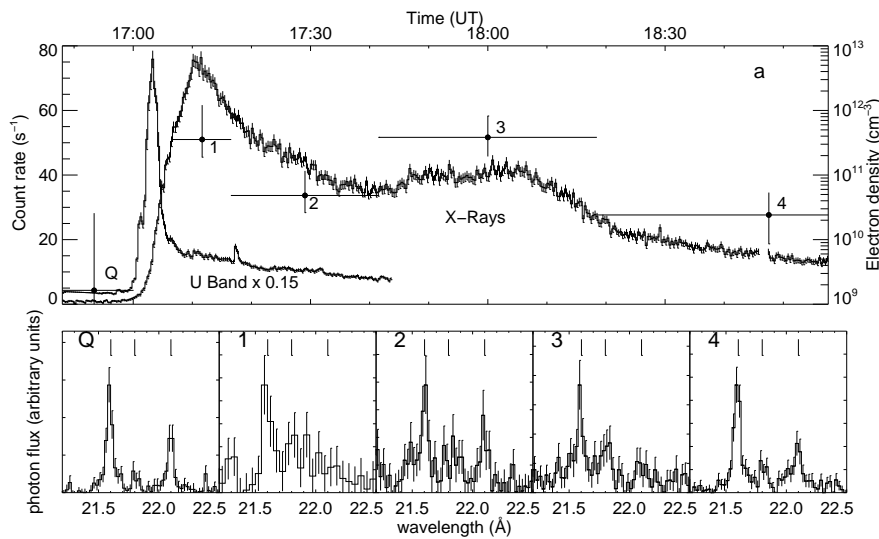


Fig. 11 Evolution of the density value during a large flare on Proxima Centauri (Güdel et al., 2002, 2004). The upper panel shows the X-ray and U-band light curves. The large crosses show electronic densities inferred from O VII, during different time intervals (the density scale is given on the right y-axis). In the bottom panel, the intensity of the three lines is shown for the five time intervals. The three marks in the upper parts of the figures show the locations of the resonance, intercombination, and forbidden lines, from left to right. Figure from Güdel and Nazé (2009). Courtesy of Astronomy and Astrophysics Review.

ing flares it can reach 10^{10} – 10^{12} cm^{-3} (e.g., Acton et al., 1972; McKenzie et al., 1980; Doschek et al., 1981; Pradhan and Shull, 1981; Wolfson et al., 1983; Linford and Wolfson, 1988; Antonucci, 1989). Figure 10 illustrates that the relative intensity ratio of intercombination and forbidden lines increases during solar flares, which corresponds to a decrease of the observed \mathcal{R} ratio. This increase of the density during the flare is consistent with the chromospheric evaporation scenario. A similar behavior has been observed during a large flare from Proxima Centauri (Güdel et al., 2002, 2004), mainly inferred from the intensity of the O VII lines (Fig. 11). The intensity of the O VII forbidden line almost tends to zero during the flare, while a strong intercombination line stands out. The inferred density value rapidly increases from a pre-flare value of $n_e < 10^{10}$ cm^{-3} to about 4×10^{11} cm^{-3} at flare peak, before declining to about 2×10^{10} cm^{-3} , then increases again during a secondary peak, followed by a gradual decay. Such increase of the density during flares has been suggested in several other stars (see the review by Güdel and Nazé 2009 and references therein).

This density diagnostic has been successfully applied to the classical T Tauri star TW Hydrae (~ 10 Myr) spectra, for which a high density value, about 10^{13} cm^{-3} , has been inferred by Kastner et al. (2002) (see also Stelzer and Schmitt 2004; Raassen 2009). These authors suggested that such a high density plasma could be located in the shock of an accretion column. This was the first time that X-rays were used to probe the accretion shock on a low-mass star. Very recently, Brickhouse et al. (2010) have reported the analysis of a very deep observation of TW Hydrae with *Chandra*/HETG (total time exposure ~ 490 ks). The use of the \mathcal{G} and \mathcal{R} ratios has allowed them to reveal three distinct regions of the stellar atmosphere: the stellar corona ($T_e \sim 10$ MK),

the accretion shock ($T_e \sim 2.5$ MK, and $n_e \sim 3 \times 10^{12} \text{ cm}^{-3}$), and a very large extended volume of warm postshock plasma ($T_e \sim 1.75$ MK, and $n_e \sim 5.7 \times 10^{11} \text{ cm}^{-3}$). High density values are also found in some active cool stars but are associated with plasma with higher temperature, $T_e \sim 10$ MK (e.g., Testa et al., 2004a), while in the case of TW Hydrae, the high density is produced at a significantly lower temperature, compatible with what is expected for accretion shocks. Such high values of the electronic density have been found in several other classical T Tauri stars (see the review by Güdel and Nazé 2009 and references therein).

We would like to notice that since the emissivity of a plasma is proportional to n_e^2 (and the volume), any determination of the density value is biased toward detections of the regions with the highest densities. Therefore, as for any other density diagnostics, the observed \mathcal{R} ratio reflects the density distribution. As shown by Güdel (2004) in cases of stellar coronae, “the inferred density is not an average over the coronal volume”, but rather describe “the steepness of the density distribution”.

In PIE plasmas, this diagnostic has also been applied to obtain information about the density value (often upper limit) for the warm absorber in active galactic nuclei between $10^9 - 10^{11} \text{ cm}^{-3}$ (e.g., NGC 4051: Collinge et al. 2001; NGC 4593: McKernan et al. 2003; NGC 4151: Schurch et al. 2004). For X-ray binaries, the S/N is in general better, allowing a more accurate determination of the line intensities, and thus on the \mathcal{R} ratio. For example, Cottam et al. (2001) found for the low-mass X-ray binary EXO 0748-67, using O VII and Ne IX, density values of $2 \times 10^{12} \text{ cm}^{-3}$ and $> 7 \times 10^{12} \text{ cm}^{-3}$, respectively (see also Jimenez-Garate et al. 2003). For the magnetic cataclysmic variable AE Aqr, Itoh et al. (2006) found a disagreement between the density value found from N VI and O VII of $\sim 10^{11} \text{ cm}^{-3}$ and the geometrical scale (inferred from the emission measure), and concluded that the plasma cannot be produced by mass accretion into the white dwarf.

4.2.2 Influence of the UV radiation field

As shown previously, the 3S_1 metastable (m) level can be depopulated to the 3P level (p_k) by collisions with electrons (but also in some cases by protons and α -particles), then increasing the relative intensity of intercombination line over that of the forbidden line. However, another atomic process can be responsible of a strong intercombination line: this is the excitation due to a UV photon (e.g., Gabriel and Jordan 1969b; Doschek and Meekins 1970; Blumenthal et al. 1972; Mewe and Schrijver 1975, 1978a; Porquet et al. 2001a; Kahn et al. 2001; Waldron and Cassinelli 2001). Indeed, the wavelengths corresponding to the 3S_1 to 3P transitions are in UV (see table 2). Therefore, a strong UV radiation field can mimic a high-density plasma. The rate (in

C v	N vI	O vII	Ne IX	Mg XI	Si XIII
2280	1906	1637	1270	1033	864

Table 2 Wavelengths in Angstrom for the UV transition between 3S_1 and 3P_1 levels that correspond to the upper levels of the forbidden line z and the intercombination line y (the dominant intercombination line for ions lighter than S xv) from C v to Si XIII (Porquet et al., 2001a).

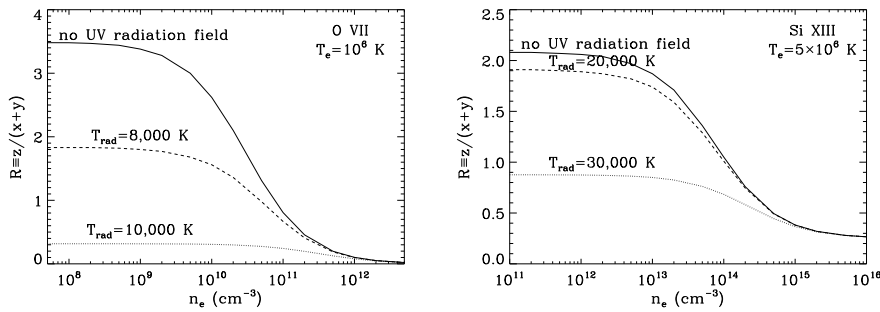


Fig. 12 Effects of UV photo-excitation on the calculated \mathcal{R} ratios for O VII and Si XIII, with a dilution factor W of 0.5. The \mathcal{R} ratio in case of no radiation field is given for comparison. *Left panel:* O VII at $T_e=10^6$ K and for two values of T_{rad} (8 000 K, and 10 000 K). *Right panel:* Si XIII at $T_e=5 \times 10^6$ K and for two values of T_{rad} (20 000 K, and 30 000 K). Calculations are from Porquet et al. (2001a).

s^{-1}) of absorption of the UV photon is:

$$B_{mp_k} = \frac{W A_{p_k m} (w_{p_k} / w_m)}{\exp\left(\frac{\Delta E_{mp_k}}{k T_{\text{rad}}}\right) - 1}, \quad (5)$$

where $A_{p_k m}$ is the spontaneous radiative decay of the p_k level ($^3P_{0,1,2}$) to the m level (3S_1), w_{p_k} and w_m are the statistical weights of the p_k and m levels, respectively, ΔE_{mp_k} is the energy between the p_k and m levels, and T_{rad} is the effective radiation temperature, i.e., the black body temperature of the radiation source, and W is the dilution factor of the radiation, defined as:

$$W = \frac{1}{2} \left[1 - \left(1 - \left(\frac{r_*}{r} \right)^2 \right)^{1/2} \right], \quad (6)$$

where r is the distance from the center of the stellar source of radius r_* . For stars such as Capella or Procyon, W is equal to 0.5, because UV from the photosphere irradiates coronal structures that are close to the stellar surface. In a binary star such as Algol the UV radiation field originates from the hot primary star that illuminates the cool secondary star, which emits the X-rays. Therefore, in this latter case W is much lower ($\simeq 0.01$). The impact of the UV radiation field is then dependent of the T_{rad} value and/or the dilution factor of the radiation.

The left panel of Fig. 12 displays the \mathcal{R} ratio for O VII (with $W=0.5$) when there is no radiation field and for two values of T_{rad} , i.e., 8 000 K and 10 000 K. The ratio decreases when the radiation field temperature increases, especially \mathcal{R}_0 . For example, an observed line ratio of about 2 corresponds to a density of a few 10^{10} cm^{-3} when the UV radiation field can be neglected, and to only an upper limit about 10^9 cm^{-3} for $T_{\text{rad}}=8 000$ K. The right panel of Fig. 12 shows that the \mathcal{R} ratio for Si XIII is sensitive to higher values of T_{rad} .

To summarize, the photo-excitation process has an important impact for low- Z ions (e.g., C V, N VI, O VII) even for moderate T_{rad} values (e.g., Mewe and Schrijver, 1978a; Porquet et al., 2001a), while for higher Z ions (e.g., Mg XI, S XV), this process becomes only important for high radiation temperature (\sim few 10 000 K), as found,

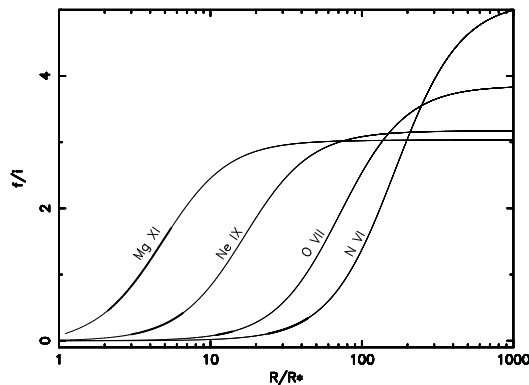


Fig. 13 The \mathcal{R} ratio values (taking into account the UV photo-excitation) versus the radial distance between the plasma where the He-like ions are formed and the UV photosphere. The present calculations, for N VI, O VII, Ne IX and Mg XI, are performed for the O star ζ Orionis assuming $T_{\text{rad}} \sim 30\,000$ K. The thickened portion of each curve shows radial distance of the X-ray plasma inferred from the measured \mathcal{R} ratio values. Figure from Raassen et al. (2008). Courtesy of Astronomy & Astrophysics.

for example, in hot (O and B) stars (e.g., Porquet et al., 2001a; Kahn et al., 2001; Waldron and Cassinelli, 2001). Indeed, Kahn et al. (2001) have found that, for the O star, ζ Puppis, the *forbidden to intercombination* line ratios within the He-like triplets are abnormally low for N VI, O VII, Ne IX, and even for Mg XI. These authors show that this is not due to a high electronic density, but rather due to the intense radiation field of this star.

At the low-density limit or when the value of the density is known, the \mathcal{R} ratio can then be used to determine the distance between the plasma where the He-like ion is found and the UV source, e.g., the radial distance from the X-ray source where the He-like ions are formed and the UV photosphere in case of stars (e.g., Kahn et al., 2001; Waldron and Cassinelli, 2001; Miller et al., 2002; Mewe et al., 2003a; Behar et al., 2004; Henley et al., 2005; Schulz et al., 2006; Leutenegger et al., 2006; Raassen et al., 2008). Figure 13 shows the \mathcal{R} ratio values (taking into account the UV photo-excitation) versus this radial distance. The present calculations, for N VI, O VII, Ne IX and Mg XI, are performed for the O star ζ Orionis assuming $T_{\text{rad}} \sim 30\,000$ K (Raassen et al., 2008). According to the UV wavelengths reported in Table 2, the flux at the wavelengths corresponding to ions up to Mg XI can be determined observationally since these are longward of the Lyman limit; while the wavelength corresponding for higher Z ions are shortward of the Lyman limit and thus must be inferred from stellar atmospheric model spectra.

For massive stars, O and early-B stars, the X-ray emission is commonly explained as produced from shocks formed by instabilities within a radiatively driven wind. He-like diagnostics can be used to discriminate two different possible geometries: (1) the spatially distributed wind shock model, where the plasma density is low and far from the UV emitting photosphere; and (2) the magnetically confined wind shock model (Babel and Montmerle, 1997), where the plasma density is high and close to the UV emitting photosphere. For example, the brightest stars of the Orion nebula's trapezium (θ^1 Ori A, C and E) shows He-like triplet emission consistent with the magnetic confinement model (Schulz et al., 2003; Gagné et al., 2005).

This ratio has been also used to infer the UV flux emitted by the accretion disk in the case of X-ray binaries, once the location and density are known (e.g., Jimenez-Garate et al., 2003).

5 Satellite lines to He-like ions

Satellite lines are lines that appear very close to or even blended with the lines of He-like and H-like ions (or other ions) and are formed by dielectronic recombination (DR) or inner-shell excitations (IE) by electrons or photons. Satellite lines have been observed in high-resolution solar spectra, as illustrated in Fig. 14. The intensity ratios of the satellite lines to resonance line can provide valuable diagnostics for the determination of electronic temperature, ionic fraction of Li-like/He-like (as well as Be-Like/He-like), and departures from Maxwellian energy distribution (see e.g., Gabriel and Jordan, 1969a; Gabriel, 1972; Gabriel and Phillips, 1979; Bely-Dubau et al., 1979, 1982; Dubau and Volonte, 1980; Lemen et al., 1984; Mewe, 1999; Oelgoetz and Pradhan, 2001). Such diagnostics will provide new diagnostic tools to probe extra-solar plasmas thanks to the gratings and calorimeters on the *Astro-H* and *IXO* satellites.

In the first laboratory observations of He-like ion resonance lines of carbon by Edlén and Tyrén (1939), some “satellite” lines appeared close to them. During the following years, Edlen and collaborators (see Edlén, 1947) obtained more He-like spectra for fluorine, magnesium and aluminium, which showed that the relative intensities of these satellite lines to the resonance line increased with nuclear charge Z . They rapidly identified them as representing the same electron transition, $1s^2 - 1s2p$, as the main line with the addition of one or possibly 2 outer electrons, e.g. $1s^2(2s) - 1s2p(2s)$. From the former identification, it was evident that some of these lines could be explained by inner-shell electron excitation of Li-like and Be-like ions by free electron collision. But it was only clear after Burgess (1964)’s famous paper that the other lines were excited by DR. The first classification of satellite lines, according to LS terms, was made by Gabriel and Jordan (1969a). But for highly ionized elements, where the fine-structure is often resolved, a new classification was proposed by Gabriel (1972), which is still used. This classification goes from a to v for the (Li-like, Be-like, ...) $n = 2$ satellite

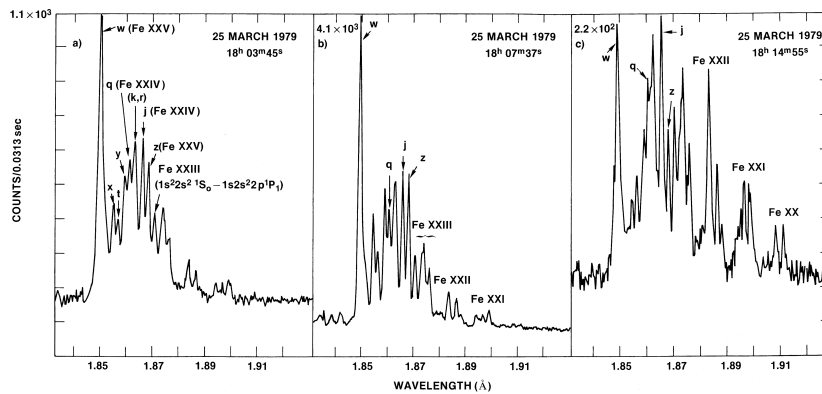


Fig. 14 Solar flare spectra of Fe XXV showing the presence of satellite lines from Fe XXIV, Fe XXIII, and Fe XXII. Figure from Doschek et al. (1979). Courtesy of Astrophysical Journal.

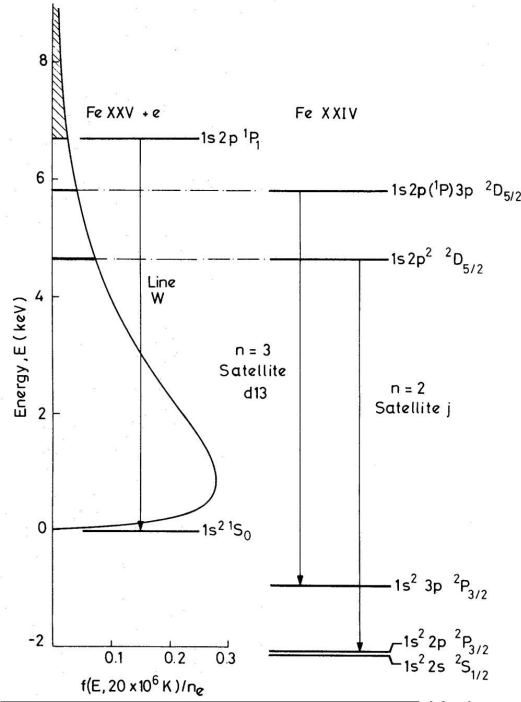


Fig. 15 Energy level diagram for the Fe XXV resonance line, w , and two dielectronic recombination satellite lines w and d_{13} . Figure from Gabriel and Phillips (1979). Courtesy of MNRAS.

lines ($1s^2 2l' - 1s 2l 2l'$) of “parent” He-like lines; w , x , y and z correspond to the parent lines, i.e., the resonance, intercombination and forbidden lines. Note that capital letters are used to define He-like satellite lines to H-like parent lines, e.g., J (see below).

Gabriel and Jordan (1969a) proposed to use intensity ratios of some satellite lines to deduce different plasma parameters such as the electronic temperature from the intensity ratio of a dielectronic line, e.g. j and k in Gabriel’s notation, to the parent resonance line w . The j and k are the strongest $n=2$ satellite lines. As an example, we shall explain the dielectronic recombination process responsible for the j line intensity, i.e., $1s^2 2p^2 P_{3/2} - 1s 2p^2^2 D_{5/2}$. The upper level of the satellite line lies well above the first ionization limit of Li-like elements, i.e., $1s^2$ and under the first excited He-like levels belonging to $1s 2s$ and $1s 2p$ configurations. Due to electron-electron repulsion, it is unstable and can decay by auto-ionization : an electron is ejected. From the energy conservation rule, the ejected electron energy ϵ can be deduced by $\epsilon = E(1s 2p^2^2 D_{5/2}) - E(1s^2 1S_0)$. In fact, from the quantum mechanics energy uncertainty relation, the possible energies ϵ are spread, with the energy width being proportional to the inverse of auto-ionizing level lifetime which contains both radiative and auto-ionization decays. And, from the micro-reversibility principle, the auto-ionization process has a reverse process called dielectronic capture (or radiationless capture). A free plasma electron with an energy inside the small ϵ width, already described, can be captured by a He-like ion in its ground level $1s^2$. The resulting auto-ionizing level subsequently decays either by auto-ionization or by radiation (if

possible). The latter possibility corresponds to the j satellite line emission, usually a “pure” dielectronic recombination line, i.e., only DR can produce the j line. The electrons contributing to the excitation of the parent line w and to the satellite line j have very distinct energy ranges. The line ratio j/w is therefore strongly temperature dependent. It is the basic principle of the diagnostic proposed in 1969. Later on, Bely-Dubau et al. (1979) calculations for $n \geq 3$ for iron He-like satellite lines, $1s2lnl - 1s^2nl$, showed that these DR satellite lines were blended with w , and therefore contributed to the observed w intensity. To correct the electronic temperature diagnostic, one has to suppress from the observed w the contribution of unresolved dielectronic satellites, to get a meaningful line ratio. This is particularly important for low electronic temperature diagnostics in CIE plasmas, i.e., much lower than the temperature of maximum formation. Thus, the resolution or not of the satellite lines to the main He-like line ions depends on the ions (Z), the spectral resolution and the n levels where the lines are formed for DR, hence their contributions must be accounted for accordingly (e.g., Gabriel and Phillips, 1979; Bely-Dubau et al., 1979; Porquet et al., 2001a; Oelgoetz and Pradhan, 2001; Phillips et al., 2008; Sylwester et al., 2008). Interestingly, though using data for which the spectral resolution was insufficient to resolve DR satellite lines, Audard et al. (2001) were the first ones to apply temperature diagnostics based on their (lack of) contribution to set a lower limit to the electronic temperature of the cool plasma of a stellar corona, Capella.

Since the upper level of satellite lines are auto-ionizing levels, most of them are populated by dielectronic recombination and it is often the dominant population process. Nevertheless, theoretical atomic calculations have shown that some auto-ionizing levels can have very small auto-ionization probabilities. This is the case for the q line, $1s^2 2s^2 S_{1/2} - 1s 2p(^1P)2s^2 P_{3/2}$, for example. Due to interaction effects between electrostatic interaction and spin-orbit, the matrix elements cancel and the auto-ionization of the q line is almost zero for Z nuclear charge close to iron ($Z = 26$). The q line is then excited only by electron collision from the Li-like ground state $1s^2 2s$ (IE). The free electron energy range for excitation being almost the same and the atomic collisional process being similar, the ratio of q over w , corrected for unresolved satellites, gives directly the abundance ratio of Li-like to He-like ions, almost independently of the electronic temperature. It is a very reliable diagnostic that was used, conjointly with the j/w or k/w ratios, to construct observational curves of relative abundances of Li-like and Be-like abundances to He-like, versus electronic temperature, for iron and calcium from solar data (e.g., Antonucci et al., 1987). Both electronic temperature and ionic abundance diagnostics were very popular in solar X-ray astronomy to study solar flares, from 1969. An exhaustive review of the solar observations made until 1979 can be found in Dubau and Volonte (1980). Since 1980, one of the most original uses of these diagnostics has been in tokamaks, to determine the electronic temperature in the plasma core where the nuclear fusion might take place.

Non-thermal electron distribution can have an impact on the atomic process rates, such as electron excitation, ionization and recombination (hence on the ionization balance): e.g., Owocki and Scudder (1983), Dzifčáková (1992), Porquet et al. (2001b), Kaastra et al. (2009), Prokhorov et al. (2009). The ratios of the satellite to resonance line are sensitive to departure from a Maxwellian electron distribution (e.g., Gabriel and Phillips, 1979; Seely et al., 1987; Mewe, 1999). Indeed the satellite lines and the resonance lines are not sensitive to the same part of the electron distribution. As shown for Fe XXV in Fig. 15, the resonance line is produced by excitation by electrons with energy above 6.701 keV, while the DR satellite lines are due to the capture of electron with an en-

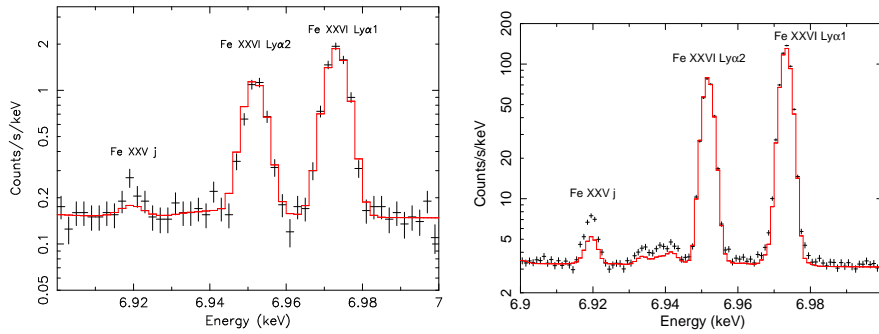


Fig. 16 *Astro-H* (left panel) and *IXO 100 ks* (right panel) simulations of the spectrum expected for a supra-thermal electron distribution behind the shock in a cluster of galaxies. The excess detection of the *J* satellite line of the He-like Fe XXV ion to the H-like Fe XXVI parent resonance lines will be significantly detected. Figures from Kaastra et al. (2009). Courtesy of Astronomy & Astrophysics.

ergy, to within the auto-ionization width ($> 10^{-4}$ keV), of 4.694 keV and 5.815 keV for the *j* and d13 satellite lines, respectively. Therefore, depending on the shape of the electron distribution, either the intensity of the satellite lines or of the resonance line will be modified compared to that expected from a Maxwellian electron distribution. In case of a Maxwellian electron distribution, the temperature inferred from satellite lines must be identical. Such diagnostics will be useful to test the departure from a Maxwellian electron distribution in , e.g., stellar flares, supernova remnants, and clusters of galaxies. As an illustration, Fig. 16 shows *Astro-H* and *IXO 100 ks* simulations of the spectrum expected for a supra-thermal electron distribution behind the shock in a cluster of galaxies, showing that the excess detection of the *J* He-like Fe XXV satellite line to the resonance line of the H-like Fe XXVI, will be significantly detected (Kaastra et al., 2009) if fit assuming an electron Maxwellian distribution. The so-called *J* He-like satellite line is composed of several satellite lines with transitions $1s2l-2l2p$ $l=s, p$ (Dubau et al., 1981). This satellite line has already been observed in solar flare spectra (Parmar et al., 1981; Tanaka, 1986; Pike et al., 1996).

In high temperature CIE plasmas, DR satellite lines are usually observed in emission for high Z and inner-shell satellite lines are even present for low Z , (e.g., Carbon spectra from Edlén and Tyrén 1939). Conversely, in the low temperature plasmas found in PIE plasmas, both dielectronic recombinations rates become negligible, hence only satellite lines formed by inner-shell photo-excitation can be significant, e.g.: the satellite lines formed by inner-shell photo-excitation of Li-like ions: $q, r, s,$ and t ($1s^22s + \text{photon} \rightarrow 1s2s2p$) and of Be-like ions: β ($1s^22s^2 + \text{photon} \rightarrow 1s2s^22p$). The two strongest satellite lines expected are q and β , though this depends upon the relative abundance of Li-like and Be-like ions, respectively. Such satellite lines have already been observed in the spectra of the Seyfert type I galaxy, NGC 5548 (Steenbrugge et al., 2003), though in absorption since in type I active galactic nuclei the so-called warm absorber/emitter that are thought to emit highly-ionized lines are seen mainly in absorption. In Figure 3 of Steenbrugge et al. (2003), one can see, close to the oxygen He-like lines (O VII), inner-shell satellite lines of Li-like (O VI) and Be-like (O V), in absorption. One must also mention that the parent O VII w line is also observed (partly) in absorption. In Seyfert 2 galaxies, the satellite lines (as for the main He-like lines) should be observed

in emission, allowing the use of the above diagnostics.

Very high-spectral resolution spectra up to an energy of 10 keV that will be obtained in the near future will allow observers to apply these diagnostics for numerous astrophysical plasmas such as stellar coronae, supernova remnants, X-ray binaries, active galactic nuclei, and clusters of galaxies.

6 Conclusions and perspectives

As reviewed here, diagnostics based on the main He-like ion lines can be very useful to determine the properties of astrophysical plasmas, such as the ionization processes (collisional excitation, recombination, charge transfer), departure from ionization equilibrium, electronic temperature, electronic density, and distance between the plasma where the He-like ions are formed and the UV radiation source (e.g., for stellar photosphere). The main advantages of the use of these close lines is that, for a given He-like ions, the line ratios are emitted in the same emitting volume, and are moreover insensitive to instrumental calibration, Galactic column density effects, and elemental abundances. These diagnostics were first applied to the solar corona for both active regions and flares. Thanks to the current generation of X-ray satellites, *Chandra* and *XMM-Newton*, these diagnostics are successfully used to probe the physical properties of extra-solar plasmas such as stellar coronae (from cool to hot stars), active galactic nuclei, X-ray binaries, and supernova remnants.

With the next generation of X-ray satellites, namely *Astro-H* and *IXO*, unprecedented spectral resolution combined with higher sensitivity will be reached. For *Astro-H* (JAXA, launch planned in 2014) with the Soft X-ray Spectrometer (SXS) aboard, a FWHM spectral resolution of at least 7 eV (with a goal to 4 eV) over the 0.3–12 keV energy range will be attained. While for *IXO* (ESA, NASA, JAXA), the planned resolving power of the grating (XGS) will be at least 3000 for the soft 0.3–1 keV energy band, and a spectral resolution of 2.5 eV for the X-ray Microcalorimeter Spectrometer (XMS) over the broad 0.3–7 keV energy range. Therefore the resonance, intercombination and forbidden lines of He-like ions will be resolved up to Ni xxvii, including Fe xxv. Therefore higher density and/or higher temperature plasmas will be probed such as, for example, in magnetic cataclysmic variables, X-ray binaries, active galactic nuclei, and galaxy clusters. The resolution of several satellite lines will permit useful diagnostics for the determination of electronic temperature, ionic fraction, departure from ionization equilibrium and from Maxwellian electron distribution. Moreover, the combination of higher spectral resolution and sensitivity will be used to determine various physical properties of numerous astrophysical objects, including weak and high-redshift ones. Then statistics of the physical properties of a certain classes of objects (active galactic nuclei, X-ray binaries, galaxy clusters, stellar corona, supernova remnants) will be performed over luminosities, types, accretion rates, and distances.

We would like to conclude this review with the following advice from Liedahl (1999): “In general, we need to bring to bear as many diagnostics as are available in order to make an internally consistent interpretation of an X-ray spectrum”.

Acknowledgements The authors would like to sincerely thank the anonymous referee for his thorough reading of this manuscript. D. P. would like to acknowledge the organizing committee for inviting her to give this review about He-like ions, and would like to dedicate this review to Rolf Mewe.

References

- L.W. Acton, W.A. Brown, Temperature and ionization balance dependence of O VII line ratios. *ApJ* **225**, 1065–1068 (1978). doi:10.1086/156574
- L.W. Acton, R.C. Catura, A.J. Meyerott, C.J. Wolfson, J.L. Culhane, Coronal survey in X-rays of O VII and Ne IX. *Solar Phys.* **26**, 183–201 (1972). doi:10.1007/BF00155119
- E. Antonucci, Solar flare spectral diagnosis - Present and future. *Solar Phys.* **121**, 31–60 (1989). doi:10.1007/BF00161686
- E. Antonucci, M.A. Dodero, A.H. Gabriel, K. Tanaka, J. Dubau, Ionization balance for iron XXV, XXIV and XXIII derived from solar flare X-ray spectra. *A&A* **180**, 263–268 (1987)
- C. Argiroffi, A. Maggio, G. Peres, J.J. Drake, J. López-Santiago, S. Sciortino, B. Stelzer, X-ray optical depth diagnostics of T Tauri accretion shocks. *A&A* **507**, 939–948 (2009). doi:10.1051/0004-6361/200912792
- M. Audard, E. Behar, M. Güdel, A.J.J. Raassen, D. Porquet, R. Mewe, C.R. Foley, G.E. Bromage, The XMM-Newton view of stellar coronae: High-resolution X-ray spectroscopy of Capella. *A&A* **365**, 329–335 (2001). doi:10.1051/0004-6361:20000246
- J. Babel, T. Montmerle, X-ray emission from Ap-Bp stars: a magnetically confined wind-shock model for IQ Aur. *A&A* **323**, 121–138 (1997)
- M.A. Bautista, T.R. Kallman, Recombination Spectra of Helium-like Ions. *ApJ* **544**, 581–591 (2000). doi:10.1086/317206
- E. Behar, M. Leutenegger, R. Doron, M. Güdel, U. Feldman, M. Audard, S.M. Kahn, Resolving X-Ray Sources from B Stars Spectroscopically: The Example of μ Leporis. *ApJL* **612**, 65–68 (2004). doi:10.1086/424485
- P. Beiersdorfer, T.W. Phillips, K.L. Wong, R.E. Marrs, D.A. Vogel, Measurement of level-specific dielectronic-recombination cross sections of heliumlike Fe XXV. *Physical Review A* **46**, 3812–3820 (1992). doi:10.1103/PhysRevA.46.3812
- P. Beiersdorfer, K.R. Boyce, G.V. Brown, H. Chen, S.M. Kahn, R.L. Kelley, M. May, R.E. Olson, F.S. Porter, C.K. Stahle, W.A. Tillotson, Laboratory Simulation of Charge Exchange-Produced X-ray Emission from Comets. *Science* **300**, 1558–1560 (2003). doi:10.1126/science.1084373
- P. Beiersdorfer, M. Bitter, M. Marion, R.E. Olson, Charge-exchange-produced K-shell x-ray emission from Ar^{16+} in a tokamak plasma with neutral-beam injection. *Physical Review A* **72**(3), 032725 (2005). doi:10.1103/PhysRevA.72.032725
- P. Beiersdorfer, G.V. Brown, J.H.T. Clementson, M. Frankel, M.F. Gu, S.M. Kahn, R. Kelley, C.A. Kilbourne, F.S. Porter, D. Thorn, E. Träbert, Survey of the K-shell emission from heliumlike ions with an X-ray microcalorimeter. *Journal of Physics Conference Series* **163**(1), 012022 (2009). doi:10.1088/1742-6596/163/1/012022
- F. Bely-Dubau, A.H. Gabriel, S. Volonte, Dielectronic satellite spectra for highly charged helium-like ions. V - Effect of total satellite contribution on the solar flare iron spectra. *MNRAS* **189**, 801–816 (1979)
- F. Bely-Dubau, P. Faucher, J. Dubau, A.H. Gabriel, Dielectronic satellite spectra for highly charged helium-like ions. VI - Iron spectra with improved inner-shell and helium-like excitation rates. *MNRAS* **198**, 239–254 (1982)

-
- A. Bhardwaj, R.F. Elsner, G. Randall Gladstone, T.E. Cravens, C.M. Lisse, K. Dennerl, G. Branduardi-Raymont, B.J. Wargelin, J. Hunter Waite, I. Robertson, N. Østgaard, P. Beiersdorfer, S.L. Snowden, V. Kharchenko, X-rays from solar system objects. *Planetary and Space Science* **55**, 1135–1189 (2007). doi:10.1016/j.pss.2006.11.009
- S. Bianchi, G. Matt, F. Nicastro, D. Porquet, J. Dubau, FeXXV and FeXXVI lines from low-velocity, photoionized gas in the X-ray spectra of active galactic nuclei. *MNRAS* **357**, 599–607 (2005). doi:10.1111/j.1365-2966.2005.08661.x
- M. Blaha, Proton Impact Excitation of Helium-like Ions in the Solar Corona. **3**, 246 (1971)
- G.R. Blumenthal, G.W.F. Drake, W.H. Tucker, Ratio of Line Intensities in Helium-Like Ions as a Density Indicator. *ApJ* **172**, 205 (1972). doi:10.1086/151340
- D. Bodewits, D.J. Christian, M. Torney, M. Dryer, C.M. Lisse, K. Dennerl, T.H. Zurbuchen, S.J. Wolk, A.G.G.M. Tielens, R. Hoekstra, Spectral analysis of the Chandra comet survey. *A&A* **469**, 1183–1195 (2007). doi:10.1051/0004-6361:20077410
- G. Branduardi-Raymont, A. Bhardwaj, R.F. Elsner, G.R. Gladstone, G. Ramsay, P. Rodriguez, R. Soria, J.H. Waite Jr., T.E. Cravens, A study of Jupiter’s aurorae with XMM-Newton. *A&A* **463**, 761–774 (2007). doi:10.1051/0004-6361:20066406
- N.S. Brickhouse, S.R. Cranmer, A.K. Dupree, G.J.M. Luna, S. Wolk, A Deep Chandra X-Ray Spectrum of the Accreting Young Star TW Hydrae. *ApJ* **710**, 1835–1847 (2010). doi:10.1088/0004-637X/710/2/1835
- A.C. Brinkman, J.S. Kaastra, R.L.J. van der Meer, A. Kinkhabwala, E. Behar, S.M. Kahn, F.B.S. Paerels, M. Sako, The soft X-ray spectrum from NGC 1068 observed with LETGS on Chandra. *A&A* **396**, 761–772 (2002). doi:10.1051/0004-6361:20020918
- G.V. Brown, P. Beiersdorfer, H. Chen, J. Clementson, M. Frankel, M.F. Gu, R.L. Kelley, C.A. Kilbourne, F.S. Porter, D.B. Thorn, B.J. Wargelin, Studies of X-ray production following charge exchange recombination between highly charged ions and neutral atoms and molecules. *Journal of Physics Conference Series* **163**(1), 012052 (2009). doi:10.1088/1742-6596/163/1/012052
- P. Bryans, E. Landi, D.W. Savin, A New Approach to Analyzing Solar Coronal Spectra and Updated Collisional Ionization Equilibrium Calculations. II. Updated Ionization Rate Coefficients. *ApJ* **691**, 1540–1559 (2009). doi:10.1088/0004-637X/691/2/1540
- A. Burgess, Delectronic Recombination and the Temperature of the Solar Corona. *ApJ* **139**, 776–780 (1964). doi:10.1086/147813
- G.X. Chen, R.K. Smith, K. Kirby, N.S. Brickhouse, B.J. Wargelin, Fully relativistic R-matrix calculation of electron impact excitation of NeIX. *Physical Review A* **74**(4), 042709 (2006). doi:10.1103/PhysRevA.74.042709
- M.J. Collinge, W.N. Brandt, S. Kaspi, D.M. Crenshaw, M. Elvis, S.B. Kraemer, C.S. Reynolds, R.M. Sambruna, B.J. Wills, High-Resolution X-Ray and Ultraviolet Spectroscopy of the Complex Intrinsic Absorption in NGC 4051 with Chandra and the Hubble Space Telescope. *ApJ* **557**, 2–17 (2001). doi:10.1086/321635
- J. Cottam, S.M. Kahn, A.C. Brinkman, J.W. den Herder, C. Erd, High-resolution spectroscopy of the low-mass X-ray binary EXO 0748-67. *A&A* **365**, 277–281 (2001). doi:10.1051/0004-6361:20000053
- T.E. Cravens, Comet Hyakutake x-ray source: Charge transfer of solar wind heavy ions. *Geophys. Res. Lett.* **24**, 105–108 (1997). doi:10.1029/96GL03780
- T.E. Cravens, X-ray Emission from Comets and Planets. *Advances in Space Research* **26**, 1443–1451 (2000). doi:10.1016/S0273-1177(00)00100-9
- K. Dennerl, X-rays from Nonmagnetic Planets. *Advances in Geosciences* **19**, 53–74

- (2009)
- K. Dennerl, J. Englhauser, J. Trümper, X-ray emissions from comets detected in the Röntgen X-ray satellite all-sky survey. *Science* **277**, 1625–1630 (1997). doi:10.1126/science.277.5332.1625
- K. Dennerl, C.M. Lisse, A. Bhardwaj, V. Burwitz, J. Englhauser, H. Gunell, M. Holmström, F. Jansen, V. Kharchenko, P.M. Rodríguez-Pascual, First observation of Mars with XMM-Newton. High resolution X-ray spectroscopy with RGS. *A&A* **451**, 709–722 (2006). doi:10.1051/0004-6361:20054253
- K.P. Dere, E. Landi, H.E. Mason, B.C. Monsignori Fossi, P.R. Young, CHIANTI - an atomic database for emission lines. *A&AS* **125**, 149–173 (1997). doi:10.1051/aas:1997368
- K.P. Dere, E. Landi, P.R. Young, G. Del Zanna, M. Landini, H.E. Mason, CHIANTI - an atomic database for emission lines. IX. Ionization rates, recombination rates, ionization equilibria for the elements hydrogen through zinc and updated atomic data. *A&A* **498**, 915–929 (2009). doi:10.1051/0004-6361/200911712
- G.A. Doschek, Solar flare X-ray spectra from the P78-1 spacecraft. *Solar Phys.* **86**, 49–58 (1983). doi:10.1007/BF00157173
- G.A. Doschek, J.F. Meekins, The Helium-Like Calcium, Silicon, and Sulfur Lines During the Decay of a Large Flare. *Solar Phys.* **13**, 220–225 (1970). doi:10.1007/BF00963954
- G.A. Doschek, R.W. Kreplin, U. Feldman, High-resolution solar flare X-ray spectra. *ApJL* **233**, 157–160 (1979). doi:10.1086/183096
- G.A. Doschek, U. Feldman, P.B. Landecker, D.L. McKenzie, High resolution solar flare X-ray spectra - The temporal behavior of electron density, temperature, and emission measure for two class M flares. *ApJ* **249**, 372–382 (1981). doi:10.1086/159294
- J.G. Doyle, F.P. Keenan, Plasma densities from the He-like ion NE IX. *A&A* **157**, 116–118 (1986)
- J. Dubau, S. Volonte, Dielectronic recombination and its applications in astronomy. *Reports on Progress in Physics* **43**, 199–251 (1980). doi:10.1088/0034-4885/43/2/002
- J. Dubau, M. Loulergue, A.H. Gabriel, L. Steenman-Clark, S. Volonte, Dielectronic satellite spectra for hydrogen-like iron in low density plasmas. *MNRAS* **195**, 705–719 (1981)
- E. Dzifčáková, The ionization balance of the Fe in the solar corona for a non-Maxwellian electron distribution function. *Solar Phys.* **140**, 247–267 (1992). doi:10.1007/BF00146312
- B. Edlén, Spectra of highly ionized atoms. *Physica* **13**, 545–554 (1947). doi:10.1016/0031-8914(47)90023-2
- B. Edlén, F. Tyrén, Atomic Energy States of an Unusual Type. *Nature* **143**, 940–941 (1939). doi:10.1038/143940a0
- K.A. Flanagan, C.R. Canizares, D. Dewey, J.C. Houck, A.C. Fredericks, M.L. Schatzenburg, T.H. Markert, D.S. Davis, Chandra High-Resolution X-Ray Spectrum of Supernova Remnant 1E 0102.2-7219. *ApJ* **605**, 230–246 (2004). doi:10.1086/382145
- G. Fritz, R.W. Kreplin, J.F. Meekins, A.E. Unzicker, H. Friedman, Solar X-Ray Spectrum from 1.9 to 25 Å. *ApJL* **148**, 133 (1967). doi:10.1086/180030
- R. Fujimoto, K. Mitsuda, D. Mccammon, Y. Takei, M. Bauer, Y. Ishisaki, S.F. Porter, H. Yamaguchi, K. Hayashida, N.Y. Yamasaki, Evidence for Solar-Wind Charge-Exchange X-Ray Emission from the Earth's Magnetosheath. *PASJ* **59**, 133–140 (2007)
- A.H. Gabriel, Dielectronic satellite spectra for highly-charged helium-like ionlines. MN-

- RAS **160**, 99 (1972)
- A.H. Gabriel, C. Jordan, Long Wavelength Satellites to the He-like Ion Resonance Lines in the Laboratory and in the Sun. *Nature* **221**, 947 (1969a). doi:10.1038/221947a0
- A.H. Gabriel, C. Jordan, Interpretation of solar helium-like ion line intensities. *MNRAS* **145**, 241 (1969b)
- A.H. Gabriel, C. Jordan, The Temperature Dependence of Line Ratios of Helium-Like Ions. *ApJ* **186**, 327–334 (1973). doi:10.1086/152502
- A.H. Gabriel, K.J.H. Phillips, Dielectronic satellite spectra for highly charged helium-like ions. IV - Iron satellite lines as a measure of non-thermal electron energy distributions. *MNRAS* **189**, 319–327 (1979)
- M. Gagné, M.E. Oksala, D.H. Cohen, S.K. Tonnesen, A. ud-Doula, S.P. Owocki, R.H.D. Townsend, J.J. MacFarlane, Chandra HETGS Multiphase Spectroscopy of the Young Magnetic O Star θ^1 Orionis C. *ApJ* **628**, 986–1005 (2005). doi:10.1086/430873
- H.R. Griem, Spontaneous Single-Photon Decay of 2^3S_{-1} in Helium-Like Ions. *ApJL* **156**, 103 (1969). doi:10.1086/180358
- Y.I. Grineva, V.I. Karev, V.V. Korneev, V.V. Krutov, S.L. Mandelstam, L.A. Vainstein, B.N. Vasilyev, I.A. Zhitnik, Solar X-Ray Spectra Observed from the ‘Intercosmos-4’ Satellite and the ‘Vertical-2’ Rocket. *Solar Phys.* **29**, 441–446 (1973). doi:10.1007/BF00150824
- M. Guainazzi, S. Bianchi, On the origin of soft X-rays in obscured AGN: answers from high-resolution spectroscopy with XMM-Newton. *MNRAS* **374**, 1290–1302 (2007). doi:10.1111/j.1365-2966.2006.11229.x
- M. Güdel, X-ray astronomy of stellar coronae. *The Astronomy and Astrophysics Review* **12**, 71–237 (2004). doi:10.1007/s00159-004-0023-2
- M. Güdel, Y. Nazé, X-ray spectroscopy of stars. *The Astronomy and Astrophysics Review*, 7 (2009). doi:10.1007/s00159-009-0022-4
- M. Güdel, M. Audard, S.L. Skinner, M.I. Horvath, X-Ray Evidence for Flare Density Variations and Continual Chromospheric Evaporation in Proxima Centauri. *ApJL* **580**, 73–76 (2002). doi:10.1086/345404
- M. Güdel, M. Audard, F. Reale, S.L. Skinner, J.L. Linsky, Flares from small to large: X-ray spectroscopy of Proxima Centauri with XMM-Newton. *A&A* **416**, 713–732 (2004). doi:10.1051/0004-6361:20031471
- D.B. Henley, I.R. Stevens, J.M. Pittard, Probing the wind-wind collision in γ^2 Velorum with high-resolution Chandra X-ray spectroscopy: evidence for sudden radiative braking and non-equilibrium ionization. *MNRAS* **356**, 1308–1326 (2005). doi:10.1111/j.1365-2966.2004.08556.x
- K. Itoh, S. Okada, M. Ishida, H. Kunieda, Density Diagnostics of the Hot Plasma in AE Aquarii with XMM-Newton. *ApJ* **639**, 397–404 (2006). doi:10.1086/499152
- M.A. Jimenez-Garate, N.S. Schulz, H.L. Marshall, Discrete X-Ray Signatures of a Photoionized Plasma above the Accretion Disk of the Neutron Star EXO 0748-676. *ApJ* **590**, 432–444 (2003). doi:10.1086/374864
- J.S. Kaastra, A.M. Bykov, N. Werner, Non-Maxwellian electron distributions in clusters of galaxies. *A&A* **503**, 373–378 (2009). doi:10.1051/0004-6361/200912492
- J.S. Kaastra, F.B.S. Paerels, F. Durret, S. Schindler, P. Richter, Thermal Radiation Processes. *Space Science Reviews* **134**, 155–190 (2008). doi:10.1007/s11214-008-9310-y
- S.M. Kahn, Soft X-ray spectroscopy of astrophysical plasmas, in *Saas-Fee Advanced Course 30: High-energy spectroscopic astrophysics*, ed. by M. Güdel & R. Walter, 2005, pp. 3–81

- S.M. Kahn, M.A. Leutenegger, J. Cottam, G. Rauw, J. Vreux, A.J.F. den Boggende, R. Mewe, M. Güdel, High resolution X-ray spectroscopy of zeta Puppis with the XMM-Newton reflection grating spectrometer. *A&A* **365**, 312–317 (2001). doi:10.1051/0004-6361:20000093
- T.R. Kallman, D. Liedahl, A. Osterheld, W. Goldstein, S. Kahn, Photoionization Equilibrium Modeling of Iron L Line Emission. *ApJ* **465**, 994 (1996). doi:10.1086/177485
- E. Källne, J. Källne, A.K. Pradhan, X-ray emission from He-like $n=2$ charge states produced in tokamak plasmas. *Physical Review A* **27**, 1476–1486 (1983). doi:10.1103/PhysRevA.27.1476
- J.H. Kastner, D.P. Huenemoerder, N.S. Schulz, C.R. Canizares, D.A. Weintraub, Evidence for Accretion: High-Resolution X-Ray Spectroscopy of the Classical T Tauri Star TW Hydrae. *ApJ* **567**, 434–440 (2002). doi:10.1086/338419
- F.P. Keenan, A.E. Kingston, D.L. McKenzie, The $l(1)S-n(1)P/1(1)S-2(1)P$ emission-line ratios in O VII as temperature diagnostics for solar flares and active regions. *ApJ* **291**, 855–857 (1985). doi:10.1086/163122
- F.P. Keenan, A.E. Kingston, S.S. Tayal, Theoretical NeIX line ratios compared to solar observations. *Solar Phys.* **94**, 85–89 (1984). doi:10.1007/BF00154809
- F.P. Keenan, S.M. McCann, R. Barnsley, J. Dunn, K.D. Evans, Electron density and temperature-sensitive X-ray-emission-line ratios for heliumlike Si XIII in the DITE tokamak. *Physical Review A* **39**, 4092–4097 (1989). doi:10.1103/PhysRevA.39.4092
- V. Kharchenko, M. Rigazio, A. Dalgarno, V.A. Krasnopolsky, Charge Abundances of the Solar Wind Ions Inferred from Cometary X-Ray Spectra. *ApJL* **585**, 73–75 (2003). doi:10.1086/374209
- A. Kinkhabwala, M. Sako, E. Behar, S.M. Kahn, F. Paerels, A.C. Brinkman, J.S. Kaastra, M.F. Gu, D.A. Liedahl, XMM-Newton Reflection Grating Spectrometer Observations of Discrete Soft X-Ray Emission Features from NGC 1068. *ApJ* **575**, 732–746 (2002). doi:10.1086/341482
- D. Koutroumpa, F. Acero, R. Lallement, J. Ballet, V. Kharchenko, OVII and OVIII line emission in the diffuse soft X-ray background: heliospheric and galactic contributions. *A&A* **475**, 901–914 (2007). doi:10.1051/0004-6361:20078271
- V.A. Krasnopolsky, J.B. Greenwood, P.C. Stancil, X-Ray and extreme ultraviolet emissions from comets. *Space Science Reviews* **113**, 271–374 (2004). doi:10.1023/B:SPAC.0000046754.75560.80
- R. Lallement, On the contribution of charge-exchange induced X-ray emission in the ISM and ICM. *A&A* **422**, 391–400 (2004). doi:10.1051/0004-6361:20035625
- J.R. Lemen, K.J.H. Phillips, R.D. Cowan, J. Hata, I.P. Grant, Inner-shell transitions of Fe XXIII and Fe XXIV in the X-ray spectra of solar flares. *A&A* **135**, 313–324 (1984)
- M.A. Leutenegger, F.B.S. Paerels, S.M. Kahn, D.H. Cohen, Measurements and Analysis of Helium-like Triplet Ratios in the X-Ray Spectra of O-Type Stars. *ApJ* **650**, 1096–1110 (2006). doi:10.1086/507147
- M.A. Leutenegger, S.P. Owocki, S.M. Kahn, F.B.S. Paerels, Evidence for the Importance of Resonance Scattering in X-Ray Emission Line Profiles of the O Star ζ Puppis. *ApJ* **659**, 642–649 (2007). doi:10.1086/512031
- D.A. Liedahl, The X-Ray Spectral Properties of Photoionized Plasma and Transient Plasmas, in *X-Ray Spectroscopy in Astrophysics*, ed. by J. van Paradijs & J. A. M. Bleeker. Lecture Notes in Physics, Berlin Springer Verlag, vol. 520, 1999, p. 189
- D.A. Liedahl, F. Paerels, Photoionization-Driven X-Ray Line Emission in Cygnus X-3.

- ApJL **468**, 33 (1996). doi:10.1086/310217
- D.A. Liedahl, S.M. Kahn, A.L. Osterheld, W.H. Goldstein, X-ray spectral signatures of photoionized plasmas. ApJL **350**, 37–40 (1990). doi:10.1086/185662
- G.A. Linford, C.J. Wolfson, Properties of an impulsive compact solar flare determined from Solar Maximum Mission X-ray measurements. ApJ **331**, 1036–1046 (1988). doi:10.1086/166620
- C.M. Lisse, K. Dennerl, J. Englhauser, M. Harden, F.E. Marshall, M.J. Mumma, R. Petre, J.P. Pye, M.J. Ricketts, J. Schmitt, J. Trumper, R.G. West, Discovery of X-ray and Extreme Ultraviolet Emission from Comet C/Hyakutake 1996 B2. Science **274**, 205–209 (1996). doi:10.1126/science.274.5285.205
- D.L. McKenzie, On coronal density measurements using a Ne IX X-ray line ratio. ApJ **296**, 294–296 (1985). doi:10.1086/163447
- D.L. McKenzie, R.M. Broussard, P.B. Landecker, H.R. Rugge, R.M. Young, G.A. Doschek, U. Feldman, Electron densities in a solar flare derived from X-ray spectra. ApJL **238**, 43–46 (1980). doi:10.1086/183254
- B. McKernan, T. Yaqoob, I.M. George, T.J. Turner, The Kinematics and Physical Conditions of the Ionized Gas in NGC 4593 from Chandra High-Energy Grating Spectroscopy. ApJ **593**, 142–159 (2003). doi:10.1086/376555
- R. Mewe, Note on the Helium-Like Ion Line Emission in Solar Plasmas. Solar Phys. **22**, 114–118 (1972). doi:10.1007/BF00145465
- R. Mewe, Atomic Physics of Hot Plasmas, in *X-Ray Spectroscopy in Astrophysics*, ed. by J. van Paradijs & J. A. M. Bleeker. Lecture Notes in Physics, Berlin Springer Verlag, vol. 520, 1999, p. 109
- R. Mewe, J. Schrijver, Computed $N = 2$ level populations in helium-like ions from CV to NiXXVII. Astrophysics and Space Science **38**, 345–352 (1975). doi:10.1007/BF00647133
- R. Mewe, J. Schrijver, Heliumlike ion line intensities. I - Stationary plasmas. II - Non-stationary plasmas. A&A **65**, 99–121 (1978a)
- R. Mewe, J. Schrijver, Heliumlike Ion Line Intensities. II Non-stationary Plasmas. A&A **65**, 115 (1978b)
- R. Mewe, J. Schrijver, Heliumlike ion line intensities. III - Results. A&AS **33**, 311–313 (1978c)
- R. Mewe, A.J.J. Raassen, J.P. Cassinelli, K.A. van der Hucht, N.A. Miller, M. Güdel, High-resolution X-ray spectroscopy of tau Scorpii (B0.2V) with XMM-Newton. A&A **398**, 203–211 (2003a). doi:10.1051/0004-6361:20021577
- R. Mewe, D. Porquet, A.J.J. Raassen, J.S. Kaastra, J. Dubau, J. Ness, Improved Line Ratio Calculations for He-like Ions **12**, 1123–1128 (2003b)
- N.A. Miller, J.P. Cassinelli, W.L. Waldron, J.J. MacFarlane, D.H. Cohen, New Challenges for Wind Shock Models: The Chandra Spectrum of the Hot Star δ Orionis. ApJ **577**, 951–960 (2002). doi:10.1086/342111
- J.U. Ness, J.H.M.M. Schmitt, M. Audard, M. Güdel, R. Mewe, Are stellar coronae optically thin in X-rays?. A systematic investigation of opacity effects. A&A **407**, 347–358 (2003a). doi:10.1051/0004-6361:20030880
- J. Ness, N.S. Brickhouse, J.J. Drake, D.P. Huenemoerder, Modeling the Ne IX Triplet Spectral Region of Capella with the Chandra and XMM-Newton Gratings. ApJ **598**, 1277–1289 (2003b). doi:10.1086/379059
- J. Oelgoetz, A.K. Pradhan, The $K\alpha$ complex of He-like iron with dielectronic satellites. MNRAS **327**, 42–46 (2001). doi:10.1046/j.1365-8711.2001.04980.x
- J. Oelgoetz, A.K. Pradhan, The 6.7-keV $K\alpha$ complex of He-like iron in transient

- plasmas. MNRAS **354**, 1093–1102 (2004). doi:10.1111/j.1365-2966.2004.08269.x
- S.P. Owocki, J.D. Scudder, The effect of a non-Maxwellian electron distribution on oxygen and iron ionization balances in the solar corona. ApJ **270**, 758–768 (1983). doi:10.1086/161167
- F.B.S. Paerels, S.M. Kahn, High-Resolution X-Ray Spectroscopy with CHANDRA and XMM-NEWTON. Annual Review of Astronomy & Astrophysics **41**, 291–342 (2003). doi:10.1146/annurev.astro.41.071601.165952
- A.N. Parmar, J.L. Culhane, C.G. Rapley, E. Antonucci, A.H. Gabriel, M. Loulergue, Observations of transitions of hydrogen-like Fe XXVI in solar flare spectra. MNRAS **197**, 29–34 (1981)
- R. Pepino, V. Kharchenko, A. Dalgarno, R. Lallement, Spectra of the X-Ray Emission Induced in the Interaction between the Solar Wind and the Heliospheric Gas. ApJ **617**, 1347–1352 (2004). doi:10.1086/425682
- K.J.H. Phillips, U. Feldman, E. Landi, *Ultraviolet and X-ray Spectroscopy of the Solar Atmosphere* (Cambridge University Press, ???, 2008)
- C.D. Pike, K.J.H. Phillips, J. Lang, A. Sterling, T. Watanabe, E. Hiei, J.L. Culhane, M. Cornille, J. Dubau, YOHKOH Observations of Fe XXVI X-Ray Line Emission from Solar Flares. ApJ **464**, 487 (1996). doi:10.1086/177338
- D. Porquet, J. Dubau, X-ray photoionized plasma diagnostics with helium-like ions. Application to warm absorber-emitter in active galactic nuclei. A&AS **143**, 495–514 (2000)
- D. Porquet, M. Arnaud, A. Decourchelle, Impacts of a power-law non-thermal electron tail on the ionization and recombination rates. A&A **373**, 1110–1124 (2001b). doi:10.1051/0004-6361:20010667
- D. Porquet, R. Mewe, J. Dubau, A.J.J. Raassen, J.S. Kaastra, Line ratios for helium-like ions: Applications to collision-dominated plasmas. A&A **376**, 1113–1122 (2001a). doi:10.1051/0004-6361:20010959
- D. Porquet, R. Mewe, J.S. Kaastra, J. Dubau, X-ray diagnostics for photo-ionized plasmas: He-like triplets, in *X-ray Spectroscopy of AGN with Chandra and XMM-Newton*, ed. by T. Boller, S. Komossa, S. Kahn, H. Kunieda, & L. Gallo, 2002, p. 285
- R.L. Porter, G.J. Ferland, Revisiting He-like X-Ray Emission-Line Plasma Diagnostics. ApJ **664**, 586–595 (2007). doi:10.1086/518882
- A.K. Pradhan, On the systematics of line ratios along the helium isoelectronic sequence. ApJ **263**, 477–482 (1982). doi:10.1086/160518
- A.K. Pradhan, Recombination-cascade X-ray spectra of highly charged helium-like ions. ApJ **288**, 824–830 (1985). doi:10.1086/162853
- A.K. Pradhan, J.M. Shull, Density and Temperature Diagnostics of X-Ray Sources - Line Ratios for Helium-Like Ions. ApJ **249**, 821 (1981). doi:10.1086/159340
- D.A. Prokhorov, F. Durret, V. Dogiel, S. Colafrancesco, An analysis of electron distributions in galaxy clusters by means of the flux ratio of iron lines FeXXV and XXVI. A&A **496**, 25–30 (2009). doi:10.1051/0004-6361/200811095
- A.J.J. Raassen, The X-ray spectrum of the classical T Tauri star TW Hydrae observed by LETGS aboard Chandra. A&A **505**, 755–762 (2009). doi:10.1051/0004-6361/200811374
- A.J.J. Raassen, K.A. van der Hucht, N.A. Miller, J.P. Cassinelli, XMM-Newton observations of zeta Orionis (O9.7 Ib): a collisional ionization equilibrium model. A&A **478**, 513–520 (2008). doi:10.1051/0004-6361:20077891
- A.P. Rasmussen, E. Behar, S.M. Kahn, J.W. den Herder, K. van der Heyden, The X-

-
- ray spectrum of the supernova remnant 1E 0102.2-7219. *A&A* **365**, 231–236 (2001). doi:10.1051/0004-6361:20000231
- D.H. Sampson, S.J. Goett, R.E.H. Clark, Electron-Impact Collision Strengths for Excitation of He-like Ions from the levels with $n = 1$ and 2 to All Singly Excited Levels with Higher $n \leq 5$. *Atomic Data and Nuclear Data Tables* **29**, 467 (1983). doi:10.1016/S0092-640X(83)80003-5
- J.T. Schmelz, J.L.R. Saba, J.C. Chauvin, K.T. Strong, Investigating the Effect of Opacity in Soft X-Ray Spectral Lines Emitted by Solar Coronal Active Regions. *ApJ* **477**, 509 (1997). doi:10.1086/303689
- N.S. Schulz, C.R. Canizares, J.C. Lee, M. Sako, The Ionized Stellar Wind in Vela X-1 during Eclipse. *ApJL* **564**, 21–25 (2002). doi:10.1086/338862
- N.S. Schulz, C. Canizares, D. Huenemoerder, K. Tibbets, X-Ray Modeling of Very Young Early-Type Stars in the Orion Trapezium: Signatures of Magnetically Confined Plasmas and Evolutionary Implications. *ApJ* **595**, 365–383 (2003). doi:10.1086/377214
- N.S. Schulz, P. Testa, D.P. Huenemoerder, K. Ishibashi, C.R. Canizares, X-Ray Variability in the Young Massive Triple θ^2 Orionis A. *ApJ* **653**, 636–646 (2006). doi:10.1086/508625
- N.J. Schurch, R.S. Warwick, R.E. Griffiths, S.M. Kahn, The complex soft X-ray spectrum of NGC 4151. *MNRAS* **350**, 1–9 (2004). doi:10.1111/j.1365-2966.2004.07632.x
- J.F. Seely, U. Feldman, G.A. Doschek, Observation of nonthermal energy distributions during the impulsive phase of solar flares. *ApJ* **319**, 541–554 (1987). doi:10.1086/165477
- R.K. Smith, J.P. Hughes, Ionization Equilibrium Timescales in Collisional Plasmas. *ApJ* **718**, 583–585 (2010). doi:10.1088/0004-637X/718/1/583
- R.K. Smith, N.S. Brickhouse, D.A. Liedahl, J.C. Raymond, Collisional Plasma Models with APEC/APED: Emission-Line Diagnostics of Hydrogen-like and Helium-like Ions. *ApJL* **556**, 91–95 (2001). doi:10.1086/322992
- R.K. Smith, G.X. Chen, K. Kirby, N.S. Brickhouse, A New Calculation of Ne IX Line Diagnostics. *ApJ* **700**, 679–683 (2009). doi:10.1088/0004-637X/700/1/679
- K.C. Steenbrugge, J.S. Kaastra, C.P. de Vries, R. Edelson, XMM-NEWTON High resolution spectroscopy of NGC 5548. *A&A* **402**, 477–486 (2003). doi:10.1051/0004-6361:20030261
- B. Stelzer, J.H.M.M. Schmitt, X-ray emission from a metal depleted accretion shock onto the classical T Tauri star TW Hya. *A&A* **418**, 687–697 (2004). doi:10.1051/0004-6361:20040041
- D.A. Swartz, M.E. Sulkanen, Helium-like Iron Line Temperature Diagnostics in Clusters of Galaxies. *ApJ* **417**, 487 (1993). doi:10.1086/173327
- J. Sylwester, B. Sylwester, K.J.H. Phillips, RESIK Observations of Helium-like Argon X-Ray Line Emission in Solar Flares. *ApJL* **681**, 117–120 (2008). doi:10.1086/590533
- K. Tanaka, Solar flare X-ray spectra of Fe XXVI and Fe XXV from the HINOTORI satellite. *PASJ* **38**, 225–249 (1986)
- P. Testa, J.J. Drake, G. Peres, The Density of Coronal Plasma in Active Stellar Coronae. *ApJ* **617**, 508–530 (2004a). doi:10.1086/422355
- P. Testa, J.J. Drake, G. Peres, E.E. DeLuca, Detection of X-Ray Resonance Scattering in Active Stellar Coronae. *ApJL* **609**, 79–82 (2004b). doi:10.1086/422747
- P. Testa, J.J. Drake, G. Peres, D.P. Huenemoerder, On X-Ray Optical Depth in the Coronae of Active Stars. *ApJ* **665**, 1349–1360 (2007). doi:10.1086/519920
- P.W. Vedder, C.R. Canizares, T.H. Markert, A.K. Pradhan, High-resolution X-ray

- spectroscopic evidence of nonequilibrium conditions in the Cygnus Loop. *ApJ* **307**, 269–274 (1986). doi:10.1086/164413
- J. Vink, X-ray High Resolution and Imaging Spectroscopy of Supernova Remnants, in *The X-ray Universe 2005*, ed. by A. Wilson. ESA Special Publication, vol. 604, 2006, p. 319
- J. Vink, J.M. Laming, M.F. Gu, A. Rasmussen, J.S. Kaastra, The Slow Temperature Equilibration behind the Shock Front of SN 1006. *ApJL* **587**, 31–34 (2003). doi:10.1086/375125
- J. Vink, J. Bleeker, J.S. Kaastra, A. Rasmussen, High resolution X-ray spectroscopy of G292.0+1.8/MSH 11-54. *Nuclear Physics B Proceedings Supplements* **132**, 62–65 (2004). doi:10.1016/j.nuclphysbps.2004.04.009
- W.L. Waldron, J.P. Cassinelli, Chandra Discovers a Very High Density X-Ray Plasma on the O Star ζ Orionis. *ApJL* **548**, 45–48 (2001). doi:10.1086/318926
- W.L. Waldron, J.P. Cassinelli, An Extensive Collection of Stellar Wind X-Ray Source Region Emission Line Parameters, Temperatures, Velocities, and Their Radial Distributions as Obtained from Chandra Observations of 17 OB Stars. *ApJ* **668**, 456–480 (2007). doi:10.1086/520919
- B.J. Wargelin, P. Beiersdorfer, G.V. Brown, EBIT charge-exchange measurements and astrophysical applications. *Canadian Journal of Physics* **86**, 151–169 (2008). doi:10.1139/P07-125
- B.J. Wargelin, P. Beiersdorfer, P.A. Neill, R.E. Olson, J.H. Scofield, Charge-Exchange Spectra of Hydrogenic and He-like Iron. *ApJ* **634**, 687–697 (2005). doi:10.1086/496874
- P.F. Winkler, G.W. Clark, T.H. Markert, K. Kalata, H.W. Schnopper, C.R. Canizares, A survey of X-ray line emission from the supernova remnant Puppis A. *ApJL* **246**, 27–31 (1981). doi:10.1086/183546
- P.S. Woźdowski, D.A. Liedahl, M. Sako, S.M. Kahn, F. Paerels, Resolving the Effects of Resonant X-Ray Line Scattering in Centaurus X-3 with Chandra. *ApJ* **582**, 959–971 (2003). doi:10.1086/344821
- C.J. Wolfson, J.W. Leibacher, J.G. Doyle, K.J.H. Phillips, X-ray line ratios from helium-like ions - Updated theory and SMM flare observations. *ApJ* **269**, 319–328 (1983). doi:10.1086/161045
- K. Wood, J. Raymond, Resonant Scattering of Emission Lines in Coronal Loops: Effects on Image Morphology and Line Ratios. *ApJ* **540**, 563–571 (2000). doi:10.1086/309336
- H. Zhang, D.H. Sampson, Collision rates for excitation of helium-like ions with inclusion of resonance effects. *ApJ Sup.* **63**, 487–514 (1987). doi:10.1086/191171
- H.L. Zhang, A.K. Pradhan, Relativistic and radiation damping effects in electron-impact excitation of highly charged ions. *Journal of Physics B Atomic Molecular Physics* **28**, 285–292 (1995). doi:10.1088/0953-4075/28/8/004